Search for new phenomena in final states with an energetic jet and large missing transverse momentum in pp collisions at √s=13 TeV using the ATLAS detector

EUROPEAN ORGANISATION FOR NUCLEAR RESEARCH (CERN)

Submitted to: Phys. Rev. D.

CERN-EP-2016-075
August 30, 2016

Search for new phenomena in final states with an energetic jet and large missing transverse momentum in pp collisions at $\sqrt{s} = 13$ TeVusing the ATLAS detector

The ATLAS Collaboration

Abstract

Results of a search for new phenomena in final states with an energetic jet and large missing transverse momentum are reported. The search uses proton–proton collision data corresponding to an integrated luminosity of 3.2 fb^{-1} at $\sqrt{s} = 13$ TeV collected in 2015 with the ATLAS detector at the Large Hadron Collider. Events are required to have at least one jet with a transverse momentum above 250 GeV and no leptons. Several signal regions are considered with increasing missing-transverse-momentum requirements between $E_{\mathrm{T}}^{\mathrm{miss}} > 250$ GeV and $E_{\mathrm{T}}^{\mathrm{miss}} > 700$ GeV. Good agreement is observed between the number of events in data and Standard Model predictions. The results are translated into exclusion limits in models with large extra spatial dimensions, pair production of weakly interacting dark-matter candidates, and the production of supersymmetric particles in several compressed scenarios.

Contents

1 Introduction

Events with an energetic jet and large missing transverse momentum $\vec{p}_{\mathrm{T}}^{\,\mathrm{miss}}$ (with magnitude $E_{\mathrm{T}}^{\mathrm{miss}}$) in the final state constitute a clean and distinctive signature in searches for new physics beyond the Standard Model (SM) at colliders. Such signatures are referred to as monojet-like in this paper. In particular, monojet (as well as monophoton and mono-W/Z) final states have been studied at the Large Hadron Collider (LHC) [1] in the context of searches for large extra spatial dimensions (LED), supersymmetry (SUSY), and weakly interacting massive particles (WIMPs) as candidates for dark matter.

The Arkani-Hamed, Dimopoulos, and Dvali (ADD) model for LED [16] explains the large difference between the electroweak unification scale at $O(10^2)$ GeV and the Planck scale $M_{\mathrm{Pl}} \sim O(10^{19})$ GeV by postulating the presence of n extra spatial dimensions of size R, and defining a fundamental Planck scale in $4 + n$ dimensions, M_D, given by ${M_{\mathrm{Pl}}}^2 \sim {M_D}^{2+n} R^n$. An appropriate choice of R for a given n yields a value of M_D at the electroweak scale. The extra spatial dimensions are compactified, resulting in a Kaluza–Klein tower of massive graviton modes. If produced in high-energy collisions in association with

an energetic jet, these graviton modes escape detection leading to a monojet-like signature in the final state.

Supersymmetry [17–25] is a theory for physics beyond the SM that naturally solves the hierarchy problem and provides a possible candidate for dark matter in the universe. SUSY enlarges the SM spectrum of particles by introducing a new supersymmetric partner (sparticle) for each particle in the SM. In particular, a new scalar field is associated with each left- or right-handed quark state and, ignoring inter-generational mixing, two squark mass eigenstates $\tilde{q}_1$ and $\tilde{q}_2$ result from the mixing of the scalar fields for a particular flavor.

In some SUSY scenarios, a significant mass difference between the two eigenstates in the bottom squark (sbottom) and top squark (stop) sectors can occur, leading to rather light sbottom $\tilde{b}_1$ and stop $\tilde{t}_1$ mass states. In addition, naturalness arguments suggest that the third generation squarks should be light, with masses below about 1 TeV [26]. In a generic supersymmetric extension of the SM that assumes R-parity conservation [27–31], sparticles are produced in pairs and the lightest supersymmetric particle (LSP) is stable. In this paper the LSP is assumed to be the lightest neutralino[1] $\tilde{\chi}_1^0$.

The results from the monojet-like analysis are interpreted in terms of searches for squark production using simplified models in compressed scenarios for which the mass difference $\Delta m \equiv m_{\tilde{q}} - m_{\tilde{\chi}_1^0}$ is small. Three separate processes are considered: stop pair production, where the stop decays to a charm quark and the LSP ($\tilde{t}_1 \to c + \tilde{\chi}_1^0$); sbottom pair production with $\tilde{b}_1 \to b + \tilde{\chi}_1^0$; and squark pair production, with $\tilde{q} \to q + \tilde{\chi}_1^0$ ($q = u, d, c, s$). For relatively small Δm, both the transverse momenta of the quark jets and the $E_{\mathrm{T}}^{\mathrm{miss}}$ in the final state are low, making it difficult to extract the signal from the large multijet background. In this study, the event selection makes use of the presence of initial-state radiation (ISR) jets to identify signal events (see Fig. 1 (left)). In this case, the squark-pair system is boosted, leading to larger $E_{\mathrm{T}}^{\mathrm{miss}}$.

A nonbaryonic dark matter component in the universe is commonly used to explain a range of astrophysical measurements (see, for example, Ref. [32] for a review). Since none of the SM particles are adequate dark matter candidates, the existence of a new particle is often hypothesized. Weakly interacting massive particles are one such class of particle candidates [33] that can be searched for at the LHC. Such a new particle would result in the correct relic density values for nonrelativistic matter in the early universe [34], as measured by the Planck [35] and WMAP [36] satellites, if its mass is between a few GeV and one TeV and if it has electroweak-scale interaction cross sections. Many new particle-physics models such as SUSY [17–25] also predict WIMPs.

In contrast to the Run-1 analyses with the monojet-like final state [37], the results of this analysis are not interpreted in terms of the effective-field-theory models [38]. Simplified models are used instead, providing a more complete framework that involves new mediator particles between the SM and the Dark Sector [39–42]. The predictions from simplified models coincide with those obtained by using an effective-field-theory approach when the mediator mass considered is above 10 TeV [43]. Here a model with an s-channel exchange of a spin-1 mediator particle with axial-vector couplings is considered, connecting the quarks to WIMPs of a Dirac fermion type. This is referred to as a leptophobic Z'-like model, and is defined by four free parameters: the WIMP mass m_χ, the mediator mass m_A, the coupling of the mediator to WIMPs (g_χ) and the flavor-universal coupling to quarks (g_q). Couplings to other SM particles

[1] Neutralinos $\tilde{\chi}_j^0$ ($j = 1, 2, 3, 4$ in the order of increasing mass) and charginos $\tilde{\chi}_j^\pm$ ($j = 1, 2$) are SUSY mass eigenstates formed from the mixing of the SUSY partners to the Higgs and electroweak gauge bosons.

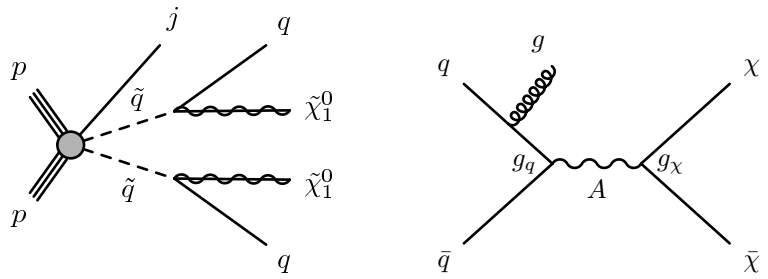

Figure 1: Left: A generic diagram for the pair production of squarks with the decay mode $\tilde{q} \to q + \tilde{\chi}_1^0$. Right: Diagram for the pair production of weakly interacting massive particles, with a leptophobic Z'-like mediator A with axial-vector couplings exchanged in the s-channel. The presence of a jet from initial-state radiation is indicated for both processes for illustration purposes.

are not allowed and the miminal mediator width is taken, defined in accord with Ref. [41] as

$$\Gamma_{\text{min}} = \frac{g_\chi^2 m_A}{12\pi}\beta_\chi^3\theta(m_A - 2m_\chi) + \sum_q \frac{3g_q^2 m_A}{12\pi}\beta_q^3\theta(m_A - 2m_q)\,, \tag{1}$$

where $\theta(x)$ denotes the Heaviside step function and $\beta_f = \sqrt{1 - \frac{4m_f^2}{m_A^2}}$ is the velocity of the fermion f with mass m_f in the mediator rest frame. The sum runs over all quark flavors. The monojet-like signature in this model emerges from initial-state radiation of a gluon as shown in Fig. 1 (right).

The paper is organized as follows. The ATLAS detector is described in the next section. Section 3 provides details of the simulations used in the analysis for background and signal processes. Section 4 discusses the reconstruction of jets, leptons, and missing transverse momentum, while Section 5 describes the event selection. The estimation of background contributions and the study of systematic uncertainties are discussed in Sections 6 and 7. The results are presented in Section 8 and are interpreted in terms of limits in models for ADD LED, SUSY in compressed scenarios, and WIMP pair production. Finally, Section 9 is devoted to the conclusions.

2 Experimental setup

The ATLAS detector [44] covers almost the whole solid angle[2] around the collision point with layers of tracking detectors, calorimeters, and muon chambers. The ATLAS inner detector covers the pseudorapidity range $|\eta| < 2.5$. It consists of a silicon pixel detector, a silicon microstrip detector, and a straw tube tracker that also measures transition radiation for particle identification, all immersed in a 2 T axial magnetic field produced by a solenoid. During the first LHC long shutdown, a new tracking layer, known as the Insertable B-Layer [45], was added at a radius of 33 mm.

[2] The ATLAS experiment uses a right-handed coordinate system with its origin at the nominal interaction point (IP) in the center of the detector and the z-axis along the beam pipe. The x-axis points from the IP to the center of the LHC ring, and the y-axis points upward. The azimuthal angle ϕ is measured around the beam axis, and the polar angle θ is measured with respect to the z-axis. The transverse energy is defined as $E_{\text{T}} = E\,\sin\theta$, the transverse momentum as $p_{\text{T}} = p\,\sin\theta$, and the pseudorapidity as $\eta = -\ln[\tan(\theta/2)]$. The rapidity is defined as $y = 0.5 \times \ln[(E + p_z)/(E - p_z)]$, where E denotes the energy and p_z is the component of the momentum along the beam direction.

High-granularity lead/liquid-argon (LAr) electromagnetic sampling calorimeters cover the pseudorapidity range $|\eta| < 3.2$. The hadronic calorimetry in the range $|\eta| < 1.7$ is provided by a steel/scintillator-tile calorimeter, consisting of a large barrel and two smaller extended barrel cylinders, one on either side of the central barrel. In the endcaps ($|\eta| > 1.5$), copper/LAr and tungsten/LAr hadronic calorimeters match the outer $|\eta|$ limits of the endcap electromagnetic calorimeters. The LAr forward calorimeters provide both the electromagnetic and hadronic energy measurements, and extend the coverage to $|\eta| < 4.9$.

The muon spectrometer measures the deflection of muons in the magnetic field provided by large superconducting air-core toroid magnets in the pseudorapidity range $|\eta| < 2.7$, instrumented with separate trigger and high-precision tracking chambers. Over most of the η range, a measurement of the track coordinates in the bending direction of the magnetic field is provided by monitored drift tubes. Cathode strip chambers with higher granularity are used in the innermost plane over $2.0 < |\eta| < 2.7$. The muon fast trigger detectors cover the pseudorapidity range $|\eta| < 2.4$ and provide a measurement of the coordinate in the non-bending plane.

The data were collected using an online two-level trigger system [46] that selects events of interest and reduces the event rate from several MHz to about 1 kHz for recording and offline processing.

3 Monte Carlo simulation

Monte Carlo (MC) simulated event samples are used to compute detector acceptance and reconstruction efficiencies, determine signal and background contributions, and estimate systematic uncertainties in the final results. Background contributions from multijet processes are determined directly from data.

3.1 Background simulation

The expected background to the monojet-like signature is dominated by $Z(\rightarrow \nu\bar{\nu})$+jets and W+jets production with $W(\rightarrow \tau\nu)$+jets being the largest W+jets background, and includes small contributions from $Z/\gamma^*(\rightarrow \ell^+\ell^-)$+jets ($\ell = e, \mu, \tau$), multijet, $t\bar{t}$, single-top, and diboson (WW, WZ, ZZ) processes. Contributions from top production associated with additional vector bosons ($t\bar{t}+W$, $t\bar{t}+Z$, or $t+Z+q/b$ processes) are negligible.

Events containing W or Z bosons with associated jets are simulated using the SHERPA-2.1.1 [47] generator. Matrix elements (ME) are calculated for up to two partons at next-to-leading order (NLO) and four partons at leading order (LO) using the Comix [48] and OpenLoops [49] matrix element generators and merged with the SHERPA parton shower (PS) [50] using the ME+PS@NLO prescription [51]. The CT10 [52] parton distribution function (PDF) set is used in conjunction with a dedicated parton shower tuning developed by the authors of SHERPA. The MC predictions are initially normalized to next-to-next-to-leading-order (NNLO) perturbative QCD (pQCD) predictions according to DYNNLO [53, 54] using MSTW2008 90% CL NNLO PDF sets [55].

For the generation of $t\bar{t}$ and single top-quarks in the Wt-channel and s-channel the POWHEG-BOX v2 [56] generator with the CT10 PDF sets in the matrix element calculations is used. Electroweak t-channel single top-quark events are generated using the POWHEG-BOX v1 generator. This generator uses the four-flavor scheme for the calculations of NLO matrix elements with the fixed four-flavor PDF set CT10. The parton shower, fragmentation, and underlying event are simulated using PYTHIA-6.428 [57]

with the CTEQ6L1 [58] PDF sets and the corresponding Perugia 2012 set of tuned parameters (P2012 tune) [59]. The top-quark mass is set to 172.5 GeV. The EvtGen v1.2.0 program [60] is used to model the decays of the bottom and charm hadrons. Finally, diboson samples (WW, WZ, and ZZ production) are generated using SHERPA-2.1.1 with CT10 PDFs and are normalized to NLO pQCD predictions [61]. The diboson samples are also generated using POWHEG interfaced to PYTHIA-8.186 and using CT10 PDFs for studies of systematic uncertainties.

3.2 Signal simulation

Simulated samples for the ADD LED model with different numbers of extra dimensions in the range $n = 2$–6 and M_D in the range 2–5 TeV are generated using PYTHIA-8.165 with NNPDF23LO [62] PDFs. The renormalization scale is set to the geometric mean of the transverse mass of the two produced particles, $\sqrt{(p_{\mathrm{T,G}}^2 + m_G^2)(p_{\mathrm{T,p}}^2 + m_p^2)}$, where m_G and $p_{\mathrm{T,G}}$ (m_p and $p_{\mathrm{T,p}}$) denote, respectively, the mass and the transverse momentum of the graviton (parton) in the final state. The factorization scale is set to the minimum transverse mass $\sqrt{m^2 + p_{\mathrm{T}}^2}$ of the graviton and the parton.

SUSY signals for stop pair production with $\tilde{t}_1 \to c + \tilde{\chi}_1^0$, for sbottom pair production decaying as $\tilde{b}_1 \to b + \tilde{\chi}_1^0$, and for the production of squark pairs from the first two squark generations with $\tilde{q} \to q + \tilde{\chi}_1^0$ ($q = u, d, c, s$) are considered. Events are generated with MG5_aMC@NLO v5.2.2.3 [63] interfaced to PYTHIA-8.186 with the ATLAS A14 [64] tune for the modeling of the squark decay, and the parton showering, hadronization, and underlying event. The matrix element calculation is performed at tree level, and includes the emission of up to two additional partons. The renormalization and factorization scales are set to the sum of transverse masses of all final state particles. The PDF used for the generation is NNPDF23LO. The ME–PS matching is done using the CKKW-L [65] prescription, with a matching scale set to one quarter of the pair-produced superpartner mass. Simulated samples with squark masses in the range between 250 GeV and 700 GeV and Δm varying between 5 GeV and 25 GeV are produced. Signal cross sections are calculated to NLO in the strong coupling constant, adding the resummation of soft gluon emission at next-to-leading-logarithmic (NLO+NLL) accuracy [66–68]. The nominal cross section and its uncertainty are taken from an envelope of cross-section predictions using different PDF sets and factorization and renormalization scales, as described in Ref. [69].

WIMP signals are simulated in POWHEG-BOX v2 [70–72] using revision 3049 of the DMV model implementation of WIMP pair production with s-channel spin-1 mediator exchange at NLO precision including parton showering effects, introduced in Ref. [73]. Renormalization and factorization scales are set to $H_{\mathrm{T}}/2$ on an event-by-event basis, where $H_{\mathrm{T}} = \sqrt{m_{\chi\chi}^2 + p_{\mathrm{T},j1}^2} + p_{\mathrm{T},j1}$ is defined by the invariant mass of the WIMP pair ($m_{\chi\chi}$) and the transverse momentum of the hardest jet ($p_{\mathrm{T},j1}$). A Breit–Wigner distribution is chosen to describe the mediator propagator. Events are generated using the NNPDF30NLO [74] parton distribution functions and interfaced to PYTHIA-8.205 with the ATLAS A14 tune for parton showering. Couplings of the mediator to WIMPs and quarks are set to $g_\chi = 1$ and $g_q = 1/4$, leading to narrow mediators with $\Gamma_{\mathrm{min}}/m_A$ up to about 5%. A grid of samples is produced for WIMP masses ranging from 1 GeV to 1 TeV and mediator masses between 10 GeV and 2 TeV.[3]

Differing pileup (multiple proton–proton interactions in the same or neighboring bunch-crossings) conditions as a function of the instantaneous luminosity are taken into account by overlaying simulated

[3] In the generation of the samples, the *bornktmin* and *bornsuppfact* MC parameters [70] are set to 150 GeV and 1 TeV, respectively, in order to suppress the generation of events at low $E_{\mathrm{T}}^{\mathrm{miss}}$.

minimum-bias events generated with PYTHIA onto the hard-scattering process. The MC-generated samples are processed with a full ATLAS detector simulation [75] based on the GEANT4 program [76]. The simulated events are reconstructed and analyzed with the same analysis chain as for the data, using the same trigger and event selection criteria.

4 Reconstruction of physics objects

Jets are reconstructed from energy deposits in the calorimeters using the anti-k_t jet algorithm [77] with the radius parameter (in y–ϕ space) set to 0.4. The measured jet transverse momentum is corrected for detector effects, including the noncompensating character of the calorimeter, by weighting energy deposits arising from electromagnetic and hadronic showers differently. In addition, jets are corrected for contributions from pileup, as described in Ref. [78]. Jets with corrected $p_{\mathrm{T}} > 20$ GeV and $|\eta| < 2.8$ are initially considered in the analysis. Track-based variables to suppress pileup jets have been developed. A combination of two such variables called the jet-vertex tagger (JVT) is constructed. In order to remove jets originating from pileup collisions, for central jets ($|\eta| < 2.4$) with $p_{\mathrm{T}} < 50$ GeV a significant fraction of the tracks associated with each jet must have an origin compatible with the primary vertex, as defined by the jet-vertex tagger [79].

The presence of leptons (electrons or muons) in the final state is used in the analysis to define control samples and to reject background contributions in the signal regions (see Sections 5 and 6). Electron candidates are initially required to have $p_{\mathrm{T}} > 20$ GeV and $|\eta| < 2.47$, and to satisfy the loose electron shower shape and track selection criteria described in Refs. [80, 81]. Overlaps between identified electrons and jets in the final state are resolved. Jets are discarded if their separation $\Delta R = \sqrt{(\Delta\eta)^2 + (\Delta\phi)^2}$ from an identified electron is less than 0.2. The electrons separated by ΔR between 0.2 and 0.4 from any remaining jet are removed.

Muon candidates are formed by combining information from the muon spectrometer and inner tracking detectors as described in Ref. [80] and are required to have $p_{\mathrm{T}} > 10$ GeV and $|\eta| < 2.5$. Jets with $p_{\mathrm{T}} > 20$ GeV and less than three tracks with $p_{\mathrm{T}} > 0.4$ GeV associated with them are discarded if their separation ΔR from an identified muon is less than 0.4. The muon is discarded if it is matched to a jet that has at least three tracks associated with it.

The $E_{\mathrm{T}}^{\mathrm{miss}}$ is reconstructed using all energy deposits in the calorimeter up to pseudorapidity $|\eta| = 4.9$. Clusters associated with either electrons or photons with $p_{\mathrm{T}} > 20$ GeV and those associated with jets with $p_{\mathrm{T}} > 20$ GeV make use of the corresponding calibrations for these objects. Softer jets and clusters not associated with these objects are calibrated using tracking information [82]. As discussed below, in this analysis the $E_{\mathrm{T}}^{\mathrm{miss}}$ is not corrected for the presence of muons in the final state.

5 Event selection

The data sample considered in this paper was collected with tracking detectors, calorimeters, muon chambers, and magnets fully operational, and corresponds to a total integrated luminosity of 3.2 fb^{-1}. The data were selected online using a trigger logic that selects events with $E_{\mathrm{T}}^{\mathrm{miss}}$ above 70 GeV, as computed at the final stage of the two-level trigger system of ATLAS. With the final analysis requirements, the trigger

selection is fully efficient for $E_{\mathrm{T}}^{\mathrm{miss}} > 250$ GeV, as determined using a data sample with muons in the final state. The following selection criteria, summarized in Table 1, are applied in the signal regions.

- Events are required to have a reconstructed primary vertex for the interaction with at least two associated tracks with $p_{\mathrm{T}} > 0.4$ GeV and consistent with the beamspot envelope; when more than one such vertex is found, the vertex with the largest summed p_{T}^2 of the associated tracks is chosen.
- Events are required to have $E_{\mathrm{T}}^{\mathrm{miss}} > 250$ GeV. The analysis selects events with a leading (highest p_{T}) jet with $p_{\mathrm{T}} > 250$ GeV and $|\eta| < 2.4$ in the final state. A maximum of four jets with $p_{\mathrm{T}} > 30$ GeV and $|\eta| < 2.8$ are allowed. A separation in the azimuthal plane of $\Delta\phi(\text{jet}, \vec{p}_{\mathrm{T}}^{\,\mathrm{miss}}) > 0.4$ between the missing transverse momentum direction and each selected jet is required. This requirement reduces the multijet background contribution where the large $E_{\mathrm{T}}^{\mathrm{miss}}$ originates mainly from jet energy mismeasurement.
- Events are rejected if they contain any jet inconsistent with the requirement that they originate from a proton–proton collision. Jet quality selection criteria [83] involve quantities such as the pulse shape of the energy depositions in the cells of the calorimeters, electromagnetic fraction in the calorimeter, calorimeter sampling fraction, or charged-particle fraction.[4] The loose criteria are applied to all jets with $p_{\mathrm{T}} > 20$ GeV and $|\eta| < 2.8$, dealing efficiently with coherent noise and electronic noise bursts in the calorimeter producing anomalous energy depositions [84]. Non-collision backgrounds, i.e. energy depositions in the calorimeters due to muons of beam-induced or cosmic-ray origin, are further suppressed by applying the tight selection criteria to the leading jet: the ratio of the jet charged-particle fraction to the calorimeter sampling fraction,[5] $f_{\mathrm{ch}}/f_{\mathrm{max}}$, is required to be larger than 0.1. These requirements have a negligible effect on the signal efficiency.
- Events with identified muons with $p_{\mathrm{T}} > 10$ GeV or electrons with $p_{\mathrm{T}} > 20$ GeV in the final state are vetoed.

Inclusive (IM1–IM7) and exclusive (EM1–EM6) signal regions are considered with increasing $E_{\mathrm{T}}^{\mathrm{miss}}$ thresholds from 250 GeV to 700 GeV (see Table 1). The use of inclusive $E_{\mathrm{T}}^{\mathrm{miss}}$ signal regions follows the Run 1 strategy, where the results are translated into model-independent cross section upper limits for the production of new physics. The use of exclusive $E_{\mathrm{T}}^{\mathrm{miss}}$ signal regions effectively explores information from the shape of the $E_{\mathrm{T}}^{\mathrm{miss}}$ distribution (see Sections 6.4 and 8) and enhances the sensitivity to the different new physics models.

6 Background estimation

The W+jets, $Z(\to \nu\bar{\nu})$+jets, $Z/\gamma^*(\to \tau^+\tau^-)$+jets, and $Z/\gamma^*(\to \mu^+\mu^-)$+jets backgrounds are constrained using MC samples normalized with data in selected control regions. The normalization factors are extracted simultaneously using a global fit that includes systematic uncertainties, to properly take into account correlations.

A $W(\to \mu\nu)$+jets control sample is used to define normalization factors for $W(\to \mu\nu)$+jets and $Z(\to \nu\bar{\nu})$+jets processes. As discussed in Section 6.4, the use of the $W(\to \mu\nu)$+jets control sample to constrain

[4] The charged-particle fraction is defined as $f_{\mathrm{ch}} = \sum p_{\mathrm{T}}^{\mathrm{track,jet}}/p_{\mathrm{T}}^{\mathrm{jet}}$, where $\sum p_{\mathrm{T}}^{\mathrm{track,jet}}$ is the scalar sum of the transverse momenta of tracks associated with the primary vertex within a cone of radius $\Delta R = 0.4$ around the jet axis, and $p_{\mathrm{T}}^{\mathrm{jet}}$ is the transverse momentum as determined from calorimetric measurements.

[5] f_{max} denotes the maximum fraction of the jet energy collected by a single calorimeter layer.

Table 1: Event selection criteria applied, as described in Section 5.

Selection criteria							
Primary vertex							
$E_{\mathrm{T}}^{\mathrm{miss}} > 250$ GeV							
Leading jet with $p_{\mathrm{T}} > 250$ GeV and $\lvert\eta\rvert < 2.4$							
At most four jets with $p_{\mathrm{T}} > 30$ GeV and $\lvert\eta\rvert < 2.8$							
$\Delta\phi(\text{jet}, \vec{p}_{\mathrm{T}}^{\,\mathrm{miss}}) > 0.4$							
Jet quality requirements							
No identified muons with $p_{\mathrm{T}} > 10$ GeV or electrons with $p_{\mathrm{T}} > 20$ GeV							
Inclusive signal region	IM1	IM2	IM3	IM4	IM5	IM6	IM7
$E_{\mathrm{T}}^{\mathrm{miss}}$ (GeV)	> 250	> 300	> 350	> 400	> 500	> 600	> 700
Exclusive signal region	EM1	EM2	EM3	EM4	EM5	EM6	
$E_{\mathrm{T}}^{\mathrm{miss}}$ (GeV)	[250–300]	[300–350]	[350–400]	[400–500]	[500–600]	[600–700]	

the normalization of the $Z(\rightarrow \nu\bar{\nu})$+jets process translates into a reduced uncertainty in the estimation of the main irreducible background contribution, due to a partial cancellation of systematic uncertainties and the statistical power of the $W(\rightarrow \mu\nu)$+jets control sample in data, which is about seven times larger than the $Z/\gamma^*(\rightarrow \mu^+\mu^-)$+jets control sample. A $W(\rightarrow e\nu)$+jets control sample is used to constrain the normalization of the $W(\rightarrow e\nu)$+jets and $W(\rightarrow \tau\nu)$+jets background processes. For the latter, this is motivated by the fact that the τ lepton in the $W(\rightarrow \tau\nu)$+jets background process mainly decays hadronically leading to a final-state topology in the detector similar to that of the $W(\rightarrow e\nu)$+jets sample. A small $Z/\gamma^*(\rightarrow \tau^+\tau^-)$+jets background contribution is also constrained using the $W(\rightarrow e\nu)$+jets control sample. Uncertainties related to the difference between W+jets and Z+jets final states, leading to potential differences in event kinematics and selection acceptances and efficiencies, are discussed in Section 7. Finally, a $Z/\gamma^*(\rightarrow \mu^+\mu^-)$+jets control sample is used to constrain the $Z/\gamma^*(\rightarrow \mu^+\mu^-)$+jets background contribution.

The remaining SM backgrounds from $Z/\gamma^*(\rightarrow e^+e^-)$+jets,[6] $t\bar{t}$, single top, and dibosons are determined using MC simulated samples, while the multijet background contribution is extracted from data. The contributions from non-collision backgrounds are estimated in data using the beam-induced background identification techniques described in Ref. [84].

The methodology and the samples used for estimating the background are summarized in Table 2. In the following subsections, details of the definition of the W/Z+jets control regions and of the data-driven determination of the multijet and beam-induced backgrounds are given. This is followed by a description of the background fits.

6.1 W/Z+jets background

Control samples in data, with identified electrons or muons in the final state and with requirements on the jet p_{T} and $E_{\mathrm{T}}^{\mathrm{miss}}$ identical to those in the signal regions, are used to determine the $W(\rightarrow \ell\nu)$+jets ($\ell = e, \mu, \tau$), $Z(\rightarrow \nu\bar{\nu})$+jets, and $Z/\gamma^*(\rightarrow \ell^+\ell^-)$+jets ($\ell = \mu, \tau$) background contributions. The $Z/\gamma^*(\rightarrow e^+e^-)$+jets background contribution is tiny and it is determined from MC simulation. The $E_{\mathrm{T}}^{\mathrm{miss}}$-based

[6] In the course of the analysis, the use of an additional $Z/\gamma^*(\rightarrow e^+e^-)$+jets control sample was explored for constraining the $Z/\gamma^*(\rightarrow e^+e^-)$+jets and $Z(\rightarrow \nu\bar{\nu})$+jets background contributions, leading to an insignificant improvement in the background determination.

Table 2: Summary of the methods and control samples used to constrain the different background contributions in the signal regions.

Background process	Method	Control sample
$Z(\to \nu\bar{\nu})$+jets	MC and control samples in data	$W(\to \mu\nu)$
$W(\to e\nu)$+jets	MC and control samples in data	$W(\to e\nu)$
$W(\to \tau\nu)$+jets	MC and control samples in data	$W(\to e\nu)$
$W(\to \mu\nu)$+jets	MC and control samples in data	$W(\to \mu\nu)$
$Z/\gamma^*(\to \mu^+\mu^-)$+jets	MC and control samples in data	$Z/\gamma^*(\to \mu^+\mu^-)$
$Z/\gamma^*(\to \tau^+\tau^-)$+jets	MC and control samples in data	$W(\to e\nu)$
$Z/\gamma^*(\to e^+e^-)$+jets	MC only	
$t\bar{t}$, single top	MC only	
Diboson	MC only	
Multijets	data-driven	
Non-collision	data-driven	

online trigger used in the analysis does not include muon information in the $E_{\mathrm{T}}^{\mathrm{miss}}$ calculation. This allows the collection of $W(\to \mu\nu)$+jets and $Z/\gamma^*(\to \mu^+\mu^-)$+jets control samples with the same trigger as for the signal regions.

A $W(\to \mu\nu)$+jets control sample is selected by requiring a muon consistent with originating from the primary vertex with $p_{\mathrm{T}} > 10$ GeV, and transverse mass in the range 30 GeV $< m_{\mathrm{T}} <$ 100 GeV. The transverse mass $m_{\mathrm{T}} = \sqrt{2p_{\mathrm{T}}^{\ell}p_{\mathrm{T}}^{\nu}[1-\cos(\phi^{\ell}-\phi^{\nu})]}$ is defined by the lepton and neutrino transverse momenta, where the (x, y) components of the neutrino momentum are taken to be the same as the corresponding $\vec{p}_{\mathrm{T}}^{\,\mathrm{miss}}$ components. Events with identified electrons in the final state are vetoed. Similarly, a $Z/\gamma^*(\to \mu^+\mu^-)$+jets control sample is selected by requiring the presence of two muons with $p_{\mathrm{T}} > 10$ GeV and invariant mass in the range 66 GeV $< m_{\mu\mu} <$ 116 GeV. In the $W(\to \mu\nu)$+jets and $Z/\gamma^*(\to \mu^+\mu^-)$+jets control regions, the $E_{\mathrm{T}}^{\mathrm{miss}}$ is not corrected for the presence of the muons in the final state, motivated by the fact that these control regions are used to estimate the $Z(\to \nu\bar{\nu})$+jets and the $Z/\gamma^*(\to \mu^+\mu^-)$+jets backgrounds, respectively, in the signal regions with no identified muons.

Finally, a $W(\to e\nu)$+jets dominated control sample is defined with an isolated electron candidate with $p_{\mathrm{T}} > 20$ GeV, selected with tight or medium selection criteria [80, 81] depending on p_{T}, and no additional identified leptons in the final state. The $E_{\mathrm{T}}^{\mathrm{miss}}$ calculation includes the contribution of the energy cluster from the identified electron in the calorimeter (no attempt is made to subtract it), since $W(\to e\nu)$+jets processes contribute to the background in the signal regions when the electron is not identified.

Monte Carlo-based scale factors, determined from the SHERPA simulation, are defined for each of the signal selections to estimate the different background contributions in the signal regions. As an illustration, in the case of the dominant $Z(\to \nu\bar{\nu})$+jets background process its contribution to a given signal region $N_{\mathrm{signal}}^{Z(\to\nu\bar{\nu})}$ is determined using the $W(\to \mu\nu)$+jets control sample in data according to

$$N_{\mathrm{signal}}^{Z(\to\nu\bar{\nu})} = (N_{W(\to\mu\nu),\mathrm{control}}^{\mathrm{data}} - N_{W(\to\mu\nu),\mathrm{control}}^{\mathrm{non-}W}) \times \frac{N_{\mathrm{signal}}^{\mathrm{MC}(Z(\to\nu\bar{\nu}))}}{N_{W(\to\mu\nu),\mathrm{control}}^{\mathrm{MC}}}, \tag{2}$$

where $N_{\mathrm{signal}}^{\mathrm{MC}(Z(\to\nu\bar{\nu}))}$ denotes the background predicted by the MC simulation in the signal region, and $N_{W(\to\mu\nu),\mathrm{control}}^{\mathrm{data}}$, $N_{W(\to\mu\nu),\mathrm{control}}^{\mathrm{MC}}$, and $N_{W(\to\mu\nu),\mathrm{control}}^{\mathrm{non-W}}$ denote, in the control region, the number of data events,

the number of $W(\rightarrow \mu\nu)$+jets candidates from MC simulation, and the non-$W(\rightarrow \mu\nu)$ background contribution, respectively. The $N^{\text{non-W}}_{W(\rightarrow\mu\nu),\text{control}}$ term refers mainly to top-quark and diboson processes, but also includes contributions from other W/Z+jets processes. Multijets and non-collision backgrounds in the control regions are negligible.

As discussed in Section 6.4, a global simultaneous likelihood fit to all the control regions is used to determine the normalization factors.

6.2 Multijets background

The multijet background with large $E_{\text{T}}^{\text{miss}}$ mainly originates from the misreconstruction of the energy of a jet in the calorimeter and to a lesser extent is due to the presence of neutrinos in the final state from heavy-flavor hadron decays. In this analysis, the multijet background is determined from data, using the jet smearing method as described in Ref. [85], which relies on the assumption that the $E_{\text{T}}^{\text{miss}}$ of multijet events is dominated by fluctuations in the jet response in the detector which can be measured in the data. For the IM1 and EM1 selections, the multijets background constitutes about 0.5% of the total background, and is negligible for the other signal regions.

6.3 Non-collision background

Non-collision backgrounds represent a significant portion of data acquired by $E_{\text{T}}^{\text{miss}}$ triggers. These backgrounds resemble the topology of monojet-like final states and a dedicated strategy with a suppression power of approximately 10^3 is needed in order to reduce these backgrounds to a sub-percent level. This is achieved by the jet quality selection criteria described in Section 5. The rate of jets due to cosmic-ray muons surviving this selection, as measured in dedicated cosmic ray datasets, is found to be negligible compared to the rate of data in the monojet-like signal regions. The main source of residual non-collision backgrounds is therefore beam-induced muons originating in the particle cascades due to beam halo protons intercepting the LHC collimators. The non-collision background is estimated using a method that identifies beam-induced muons based on the spatial matching of calorimeter clusters to muon track segments, reconstructed in the muon-system endcaps and pointing in a direction nearly parallel to the beam pipe [84]. The number of events where the reconstructed objects satisfy the identification criteria is corrected for the efficiency of this method. The efficiency is evaluated in a dedicated beam-induced background-enhanced region defined by inverting the tight jet quality selection imposed on the leading jet.

The results indicate an almost negligible contribution from non-collision backgrounds in the signal regions. As an example, 110 and 19 non-collision background events are estimated in the IM1 and EM3 signal regions, respectively, with no sign of non-collision backgrounds at $E_{\text{T}}^{\text{miss}} > 500$ GeV. This constitutes about 0.5% of the total background for the IM1 and EM3 selections.

6.4 Background fits

The use of control regions to constrain the normalization of the dominant background contributions from $Z(\rightarrow \nu\bar{\nu})$+jets and W+jets significantly reduces the relatively large theoretical and experimental systematic uncertainties, of the order of 20%–40%, associated with purely MC-based background predictions

in the signal regions. A complete study of systematic uncertainties is carried out, as detailed in Section 7. To determine the final uncertainty in the total background, all systematic uncertainties are treated as nuisance parameters with Gaussian shapes in a fit based on the profile likelihood method [86] and which takes into account correlations among systematic variations. The likelihood also takes into account cross-contamination between different background sources in the control regions.

A simultaneous likelihood fit to the $W(\rightarrow \mu\nu)$+jets, $W(\rightarrow e\nu)$+jets, and $Z/\gamma^*(\rightarrow \mu^+\mu^-)$+jets control regions is performed to normalize and constrain the corresponding background estimates in the signal regions. Background-only fits are performed separately in each of the inclusive regions IM1–IM7, as described in Section 5. In addition, a fit simultaneously using all the exclusive $E_{\mathrm{T}}^{\mathrm{miss}}$ regions EM1–EM6 and IM7 is performed. In this case, normalization factors are considered separately in each exclusive $E_{\mathrm{T}}^{\mathrm{miss}}$ region, which effectively employs information from the shape of the $E_{\mathrm{T}}^{\mathrm{miss}}$ distribution to enhance the sensitivity of the analysis to the presence of new phenomena.

The results of the background-only fit in the control regions are presented in detail in Table 3 for the IM1 selection. Tables 4–6 collect the results for the total background predictions in each of the control regions for the inclusive and exclusive $E_{\mathrm{T}}^{\mathrm{miss}}$ selections. As the tables indicate, the W/Z+jets background predictions receive multiplicative normalization factors that vary in the range between 0.8 and 1.2, depending on the process and the kinematic selection. Good agreement is observed between the normalization factors obtained by using inclusive or exclusive $E_{\mathrm{T}}^{\mathrm{miss}}$ regions.

Table 3: Data and background predictions in the control regions before and after the fit is performed for the IM1 selection. The background predictions include both the statistical and systematic uncertainties. The individual uncertainties are correlated, and do not necessarily add in quadrature to the total background uncertainty.

IM1 control regions	$W(\rightarrow e\nu)$	$W(\rightarrow \mu\nu)$	$Z/\gamma^*(\rightarrow \mu^+\mu^-)$
Observed events (3.2 fb^{-1})	3559	10481	1488
SM prediction (post-fit)	3559 ± 60	10480 ± 100	1488 ± 39
Fitted $W(\rightarrow e\nu)$	2410 ± 140	0.4 ± 0.1	–
Fitted $W(\rightarrow \mu\nu)$	2.4 ± 0.3	8550 ± 330	1.8 ± 0.3
Fitted $W(\rightarrow \tau\nu)$	462 ± 27	435 ± 28	0.14 ± 0.02
Fitted $Z/\gamma^*(\rightarrow e^+e^-)$	0.5 ± 0.1	–	–
Fitted $Z/\gamma^*(\rightarrow \mu^+\mu^-)$	0.02 ± 0.02	143 ± 10	1395 ± 41
Fitted $Z/\gamma^*(\rightarrow \tau^+\tau^-)$	30 ± 2	22 ± 4	0.5 ± 0.1
Fitted $Z(\rightarrow \nu\bar{\nu})$	1.8 ± 0.1	2.3 ± 0.2	–
Expected $t\bar{t}$, single top	500 ± 150	1060 ± 330	42 ± 13
Expected dibosons	150 ± 13	260 ± 25	48 ± 5
MC exp. SM events	3990 ± 320	10500 ± 710	1520 ± 98
Fit input $W(\rightarrow e\nu)$	2770 ± 210	0.4 ± 0.1	–
Fit input $W(\rightarrow \mu\nu)$	2.4 ± 0.3	8500 ± 520	1.8 ± 0.2
Fit input $W(\rightarrow \tau\nu)$	531 ± 39	500 ± 34	0.16 ± 0.03
Fit input $Z/\gamma^*(\rightarrow e^+e^-)$	0.5 ± 0.1	–	–
Fit input $Z/\gamma^*(\rightarrow \mu^+\mu^-)$	0.02 ± 0.02	146 ± 13	1427 ± 92
Fit input $Z/\gamma^*(\rightarrow \tau^+\tau^-)$	34 ± 3	25 ± 4	0.6 ± 0.1
Fit input $Z(\rightarrow \nu\bar{\nu})$	1.8 ± 0.1	2.2 ± 0.1	–
Fit input $t\bar{t}$, single top	500 ± 160	1060 ± 340	42 ± 13
Fit input dibosons	150 ± 13	260 ± 25	48 ± 5

Table 4: Data and SM background prediction, before and after the fit, in the $W(\rightarrow e\nu)$ control region for the different selections. For the SM predictions both the statistical and systematic uncertainties are included.

Inclusive Selection	IM1	IM2	IM3	IM4	IM5	IM6	IM7
Observed events (3.2 fb^{-1})	3559	1866	992	532	183	72	32
SM prediction (post-fit)	3559 ± 60	1866 ± 43	992 ± 32	532 ± 23	183 ± 14	72 ± 8	32 ± 6
SM prediction (pre-fit)	3990 ± 320	2110 ± 170	1142 ± 94	654 ± 54	216 ± 19	85 ± 8	34 ± 3
Exclusive Selection	EM1	EM2	EM3	EM4	EM5	EM6	
Observed events (3.2 fb^{-1})	1693	874	460	349	111	40	
SM prediction (post-fit)	1693 ± 41	874 ± 30	460 ± 21	349 ± 19	111 ± 11	40 ± 6	
SM prediction (pre-fit)	1880 ± 150	971 ± 79	488 ± 40	439 ± 36	131 ± 12	50 ± 5	

Table 5: Data and SM background prediction, before and after the fit, in the $W(\rightarrow \mu\nu)$ control region for the different selections. For the SM predictions both the statistical and systematic uncertainties are included.

Inclusive Selection	IM1	IM2	IM3	IM4	IM5	IM6	IM7
Observed events (3.2 fb^{-1})	10481	6279	3538	1939	677	261	95
SM prediction (post-fit)	10480 ± 100	6279 ± 79	3538 ± 60	1939 ± 44	677 ± 26	261 ± 16	95 ± 10
SM prediction (pre-fit)	10500 ± 710	6350 ± 460	3560 ± 280	2010 ± 160	700 ± 57	256 ± 23	106 ± 9
Exclusive Selection	EM1	EM2	EM3	EM4	EM5	EM6	
Observed events (3.2 fb^{-1})	4202	2741	1599	1262	416	166	
SM prediction (post-fit)	4202 ± 65	2741 ± 52	1599 ± 40	1262 ± 36	416 ± 20	166 ± 13	
SM prediction (pre-fit)	4140 ± 260	2800 ± 190	1540 ± 120	1310 ± 100	444 ± 35	150 ± 14	

Table 6: Data and SM background prediction, before and after the fit, in the $Z/\gamma^*(\rightarrow \mu^+\mu^-)$ control region for the different selections. For the SM predictions both the statistical and systematic uncertainties are included.

Inclusive Selection	IM1	IM2	IM3	IM4	IM5	IM6	IM7
Observed events (3.2 fb^{-1})	1488	877	505	293	100	33	15
SM prediction (post-fit)	1488 ± 39	877 ± 30	505 ± 22	293 ± 17	100 ± 10	33 ± 6	15 ± 4
SM prediction (pre-fit)	1520 ± 98	910 ± 59	487 ± 34	271 ± 19	89 ± 7	32 ± 3	13 ± 1
Exclusive Selection	EM1	EM2	EM3	EM4	EM5	EM6	
Observed events (3.2 fb^{-1})	611	372	212	193	67	18	
SM prediction (post-fit)	611 ± 25	372 ± 19	212 ± 15	193 ± 14	67 ± 8	18 ± 4	
SM prediction (pre-fit)	610 ± 42	422 ± 36	217 ± 15	182 ± 13	57 ± 4	19 ± 2	

Figure 2 shows, for the IM1 monojet-like kinematic selection and in the different control regions, the distributions of the $E_{\mathrm{T}}^{\mathrm{miss}}$ and the leading-jet p_{T} in data and MC simulation. The MC predictions include data-driven normalization factors as extracted from the global fit that considers exclusive $E_{\mathrm{T}}^{\mathrm{miss}}$ bins. Altogether, the MC simulation provides a good description of the shape of the measured distributions in the different control regions.

In the analysis, the control regions are defined using the same requirements for $E_{\mathrm{T}}^{\mathrm{miss}}$, leading jet p_{T}, event topologies, and jet vetoes as in the signal regions, such that no extrapolation in $E_{\mathrm{T}}^{\mathrm{miss}}$ or jet p_{T} is needed from control to signal regions. Agreement between data and background predictions is confirmed in a low-p_{T} validation region defined using the same monojet-like selection criteria with $E_{\mathrm{T}}^{\mathrm{miss}}$ limited to the range 150–250 GeV.

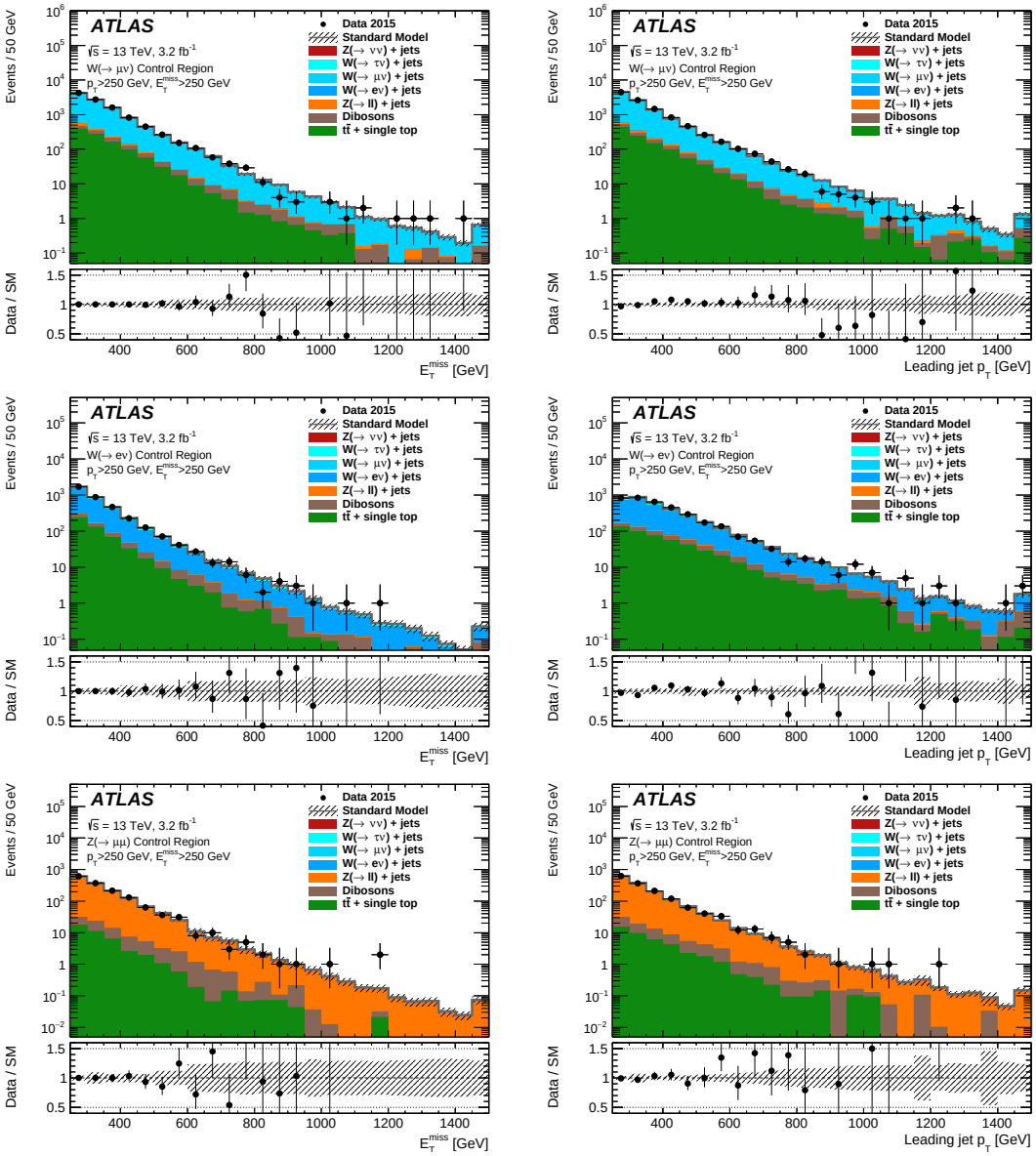

Figure 2: The measured $E_{\mathrm{T}}^{\mathrm{miss}}$ and leading-jet p_{T} distributions in the $W(\rightarrow \mu\nu)$+jets (top), $W(\rightarrow e\nu)$+jets (middle), and $Z/\gamma^{*}(\rightarrow \mu^{+}\mu^{-})$+jets (bottom) control regions, for the IM1 selection, compared to the background predictions. The latter include the global normalization factors extracted from the fit as performed in exclusive $E_{\mathrm{T}}^{\mathrm{miss}}$ bins. The error bands in the ratios include the statistical and experimental uncertainties in the background predictions as determined by the global fit to the data in the control regions. The contributions from multijets and non-collision backgrounds are negligible and are not shown in the figures.

7 Systematic uncertainties

In this section the impact of each source of systematic uncertainty on the total background prediction in the signal regions, as determined via the global fits explained in Section 6.4, is discussed. Here, the case of the inclusive $E_{\mathrm{T}}^{\mathrm{miss}}$ selections is presented. Similar studies are carried out in exclusive $E_{\mathrm{T}}^{\mathrm{miss}}$ bins.

The correlation of systematic uncertainties across $E_{\mathrm{T}}^{\mathrm{miss}}$ bins is properly taken into account. Finally, the experimental and theoretical uncertainties in the signal yields are discussed.

7.1 Background systematic uncertainties

Uncertainties in the absolute jet and $E_{\mathrm{T}}^{\mathrm{miss}}$ energy scales and resolutions [78] translate into an uncertainty in the total background which varies between ±0.5% for IM1 and ±1.6% for IM7. Uncertainties related to jet quality requirements, pileup description and corrections to the jet p_{T} and $E_{\mathrm{T}}^{\mathrm{miss}}$ introduce a ±0.2% to ±0.9% uncertainty in the background predictions. Uncertainties in the simulated lepton identification and reconstruction efficiencies, energy/momentum scale and resolution translate into an uncertainty in the total background which varies between ±0.1% and ±1.4% for the IM1 and between ±0.1% and ±2.6% for the IM7 selections, respectively.

Variations of the renormalization, factorization, and parton-shower matching scales and PDFs in the SHERPA W/Z+jets background samples translate into a ±1.1% to ±1.3% uncertainty in the total background. Model uncertainties, related to potential differences between W+jets and Z+jets final states, affecting the normalization of the dominant $Z(\rightarrow \nu\bar{\nu})$+jets background and the small $Z/\gamma^{*}(\rightarrow \tau^{+}\tau^{-})$+jets background contribution as determined in $W(\rightarrow \mu\nu)$+jets and $W(\rightarrow e\nu)$+jets control regions, are studied in detail. This includes uncertainties related to PDFs and renormalization and factorization scale settings, the parton-shower parameters and the hadronization model used in the MC simulation, and the dependence on the lepton reconstruction and acceptance. As a result, an additional ±3% uncertainty in the $Z(\rightarrow \nu\bar{\nu})$+jets and $Z/\gamma^{*}(\rightarrow \tau^{+}\tau^{-})$+jets contributions is included for all the selections. In addition, the effect from NLO electroweak corrections on the W+jets to Z+jets ratio is taken into account [87–89]. Dedicated parton-level calculations are performed with the same $E_{\mathrm{T}}^{\mathrm{miss}}$ and leading-jet-p_{T} requirements as in the IM1–IM7 signal regions. The studies suggest an effect on the W+jets to Z+jets ratio which varies between about ±1.9% for IM1 and ±5.2% for IM7, although the calculations suffer from large uncertainties, mainly due to our limited knowledge of the photon PDFs in the proton. In this analysis, these results are adopted as an additional uncertainty in the $Z(\rightarrow \nu\bar{\nu})$+jets and $Z/\gamma^{*}(\rightarrow \tau^{+}\tau^{-})$+jets contributions. Altogether, this translates into an uncertainty in the total background which varies from ±2.0% and ±3.0% for the IM1 and IM5 selections, respectively, to about ±3.9% for the IM7 selection.

Theoretical uncertainties in the predicted background yields for top-quark-related processes include: uncertainties on the absolute $t\bar{t}$ and single-top production cross sections; variations in the set of parameters that govern the parton showers and the amount of initial- and final-state soft gluon radiation; and uncertainties due to the choice of renormalization and factorization scales and PDFs. This introduces an uncertainty in the total background prediction which varies between ±2.7% and ±3.3% for the IM1 and IM7 selections, respectively. Uncertainties in the diboson contribution are estimated using different MC generators and translate into an uncertainty in the total background in the range between ±0.05% and ±0.4%. A ±100% uncertainty in the multijet and non-collision background estimations is adopted, leading to a ±0.2% uncertainty in the total background for the IM1 selection. Statistical uncertainties related to the data control regions and simulation samples lead to an additional uncertainty in the final background estimates in the signal regions which varies between ±2.5% for the IM1 and ±10% for the IM7 selections. Finally, the impact of the uncertainty in the integrated luminosity, which partially cancels in the data-driven determination of the SM background, is negligible.

7.2 Signal systematic uncertainties

Several sources of systematic uncertainty in the predicted signal yields are considered for each of the models of new physics. The uncertainties are computed separately for each signal region by varying the model parameters (see Section 8).

Experimental uncertainties include: those related to the jet and $E_{\mathrm{T}}^{\mathrm{miss}}$ reconstruction, energy scales and resolutions; and the ±5% uncertainty in the integrated luminosity, derived following a methodology similar to that detailed in Ref. [90], from a calibration of the luminosity scale using x–y beam-separation scans performed in August 2015. Other uncertainties related to the jet quality requirements are negligible ($< 1\%$).

Uncertainties affecting the signal acceptance, related to the generation of the signal samples, include: uncertainties in the modeling of the initial- and final-state gluon radiation, as determined using simulated samples with modified parton-shower parameters (by factors of two or one half) that enhance or suppress the parton radiation; uncertainties due to PDF and variations of the $\alpha_{\mathrm{s}}(m_Z)$ value employed, as computed from the envelope of CT10, MMHT2014 [91] and NNPDF30 error sets; and the choice of renormalization and factorization scales. In addition, theoretical uncertainties in the predicted cross sections, including PDF and renormalization and factorization scale uncertainties, are computed separately for the different models.

8 Results and interpretation

The number of events in data and the expected background predictions in several inclusive and exclusive signal regions, as determined using the global fit discussed in Section 6.4, are presented in detail in Table 7. The results for all the signal regions are summarized in Table 8. Good agreement is observed between the data and the SM predictions in each case. The SM predictions for the inclusive selections are determined with a total uncertainty of ±4.0%, ±6.8%, and ±12% for the IM1, IM5, and IM7 signal regions, respectively, which include correlations between uncertainties in the individual background contributions.

Figure 3 shows several measured distributions compared to the SM predictions for $E_{\mathrm{T}}^{\mathrm{miss}} > 250$ GeV, for which the normalization factors applied to the MC predictions, and the related uncertainties, are determined from the global fit carried out in exclusive $E_{\mathrm{T}}^{\mathrm{miss}}$ bins. For illustration purposes, the distributions include the impact of different ADD, SUSY, and WIMP scenarios.

The level of agreement between the data and the SM predictions for the total number of events in the different inclusive signal regions IM1–IM7 is translated into upper limits for the presence of new phenomena. A simultaneous likelihood fit is performed in both the control and signal regions, separately for each of the inclusive regions IM1–IM7. As a result, model-independent 95% confidence level (CL) upper limits on the visible cross section, defined as the production cross section times acceptance times efficiency $\sigma \times A \times \epsilon$, are extracted using the CL_s modified frequentist approach [92] and considering the systematic uncertainties in the SM backgrounds and the uncertainty in the integrated luminosity. The results are presented in Table 9. Values of $\sigma \times A \times \epsilon$ above 553 fb (for IM1) and above 19 fb (for IM7) are excluded at 95% CL. Typical event selection efficiencies ϵ varying from about 100% for IM1 to 96% for IM7 are found in simulated $Z(\rightarrow \nu\bar{\nu})$+jets background processes.

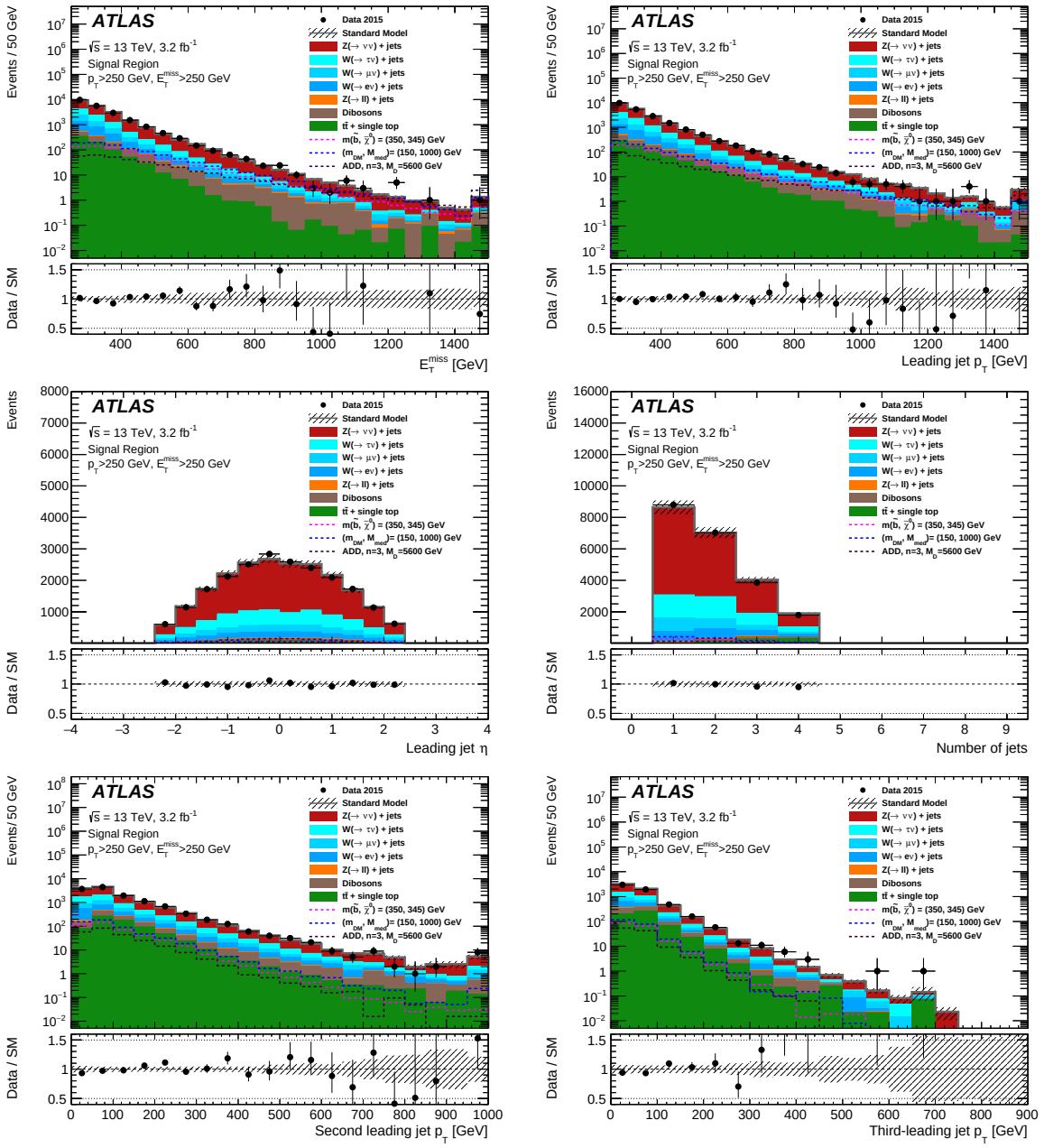

Figure 3: Measured distributions of the $E_{\mathrm{T}}^{\mathrm{miss}}$, leading-jet p_{T}, leading-jet η, jet multiplicity, second-leading-jet p_{T}, and third-leading-jet p_{T} for the IM1 selection compared to the SM predictions. The latter are normalized with normalization factors as determined by the global fit that considers exclusive $E_{\mathrm{T}}^{\mathrm{miss}}$ regions. For illustration purposes, the distributions of different ADD, SUSY, and WIMP scenarios are included. The error bands in the ratios shown in the lower panels include both the statistical and systematic uncertainties in the background predictions. The contributions from multijets and non-collision backgrounds are negligible and not shown in the figures.

Table 7: Data and SM background predictions in the signal region for several inclusive and exclusive $E_{\mathrm{T}}^{\mathrm{miss}}$ selections. For the SM prediction both the statistical and systematic uncertainties are included. In each signal region, the individual uncertainties for the different background processes can be correlated, and do not necessarily add in quadrature to the total background uncertainty.

Signal Region	IM1	EM3	EM5	IM7
Observed events (3.2 fb^{-1})	21447	2939	747	185
SM prediction	21730 ± 940	3210 ± 170	686 ± 50	167 ± 20
$W(\rightarrow e\nu)$	1710 ± 170	228 ± 26	37 ± 7	7 ± 2
$W(\rightarrow \mu\nu)$	1950 ± 170	263 ± 28	44 ± 8	11 ± 2
$W(\rightarrow \tau\nu)$	3980 ± 310	551 ± 47	101 ± 15	19 ± 4
$Z/\gamma^*(\rightarrow e^+e^-)$	0.01 ± 0.01	–	–	–
$Z/\gamma^*(\rightarrow \mu^+\mu^-)$	76 ± 30	9 ± 5	5 ± 2	2 ± 1
$Z/\gamma^*(\rightarrow \tau^+\tau^-)$	48 ± 7	5 ± 1	0.9 ± 0.2	0.2 ± 0.1
$Z(\rightarrow \nu\bar{\nu})$	12520 ± 700	1940 ± 130	443 ± 42	109 ± 18
$t\bar{t}$, single top	780 ± 240	108 ± 32	19 ± 7	3 ± 1
Dibosons	506 ± 48	82 ± 8	36 ± 5	15 ± 2
Multijets	51 ± 50	6 ± 6	1 ± 1	0.4 ± 0.4
Non-collision background	110 ± 110	19 ± 19	–	–

Table 8: Data and SM background predictions in the signal region for the different selections. For the SM predictions both the statistical and systematic uncertainties are included.

Signal Region	IM1	IM2	IM3	IM4	IM5	IM6	IM7
Observed events (3.2 fb^{-1})	21447	11975	6433	3494	1170	423	185
SM prediction	21730 ± 940	12340 ± 570	6570 ± 340	3390 ± 200	1125 ± 77	441 ± 39	167 ± 20
Signal Region	EM1	EM2	EM3	EM4	EM5	EM6	
Observed events (3.2 fb^{-1})	9472	5542	2939	2324	747	238	
SM prediction	9400 ± 410	5770 ± 260	3210 ± 170	2260 ± 140	686 ± 50	271 ± 28	

Table 9: Observed and expected 95% CL upper limits on the number of signal events, S_{obs}^{95} and S_{exp}^{95}, and on the visible cross section, defined as the product of cross section, acceptance and efficiency, $\langle\sigma\rangle_{\mathrm{obs}}^{95}$, for the IM1–IM7 selections.

Signal channel	$\langle\sigma\rangle_{\mathrm{obs}}^{95}$ [fb]	S_{obs}^{95}	S_{exp}^{95}
IM1	553	1773	1864^{+829}_{-548}
IM2	308	988	1178^{+541}_{-348}
IM3	196	630	694^{+308}_{-204}
IM4	153	491	401^{+168}_{-113}
IM5	61	196	164^{+63}_{-45}
IM6	23	75	84^{+32}_{-23}
IM7	19	61	48^{+18}_{-13}

8.1 Large extra spatial dimensions

The level of agreement between the data and the SM predictions is translated into limits on the parameters of the ADD model. Only the signal regions with $E_{\mathrm{T}}^{\mathrm{miss}} > 400$ GeV, where the SM background is moderate

and the shape difference between signal and the SM background becomes apparent, have an impact on the ADD limits. The typical $A \times \epsilon$ of the selection criteria varies, as the number of extra dimensions n increases from $n = 2$ to $n = 6$, between 5.5% and 6.6% for IM4 and between 2.9% and 4.2% for IM7.

The experimental uncertainties related to the jet and $E_{\mathrm{T}}^{\mathrm{miss}}$ scales and resolutions introduce uncertainties in the signal yields which vary between ±1% and ±3%. The uncertainties related to the modeling of the initial- and final-state gluon radiation translate into uncertainties in the ADD signal acceptance which vary between ±7% and ±10%. The uncertainties due to the PDFs, affecting the predicted signal cross sections, increase from ±16% at $n = 2$ to ±42% at $n = 6$. The effect of PDF uncertainties on the acceptance is between ±10% and ±20%, mildly increasing with increasing n and $E_{\mathrm{T}}^{\mathrm{miss}}$. Similarly, the variations of the renormalization and factorization scales introduce a ±23% to ±36% uncertainty in the signal yields, with increasing n and $E_{\mathrm{T}}^{\mathrm{miss}}$ requirements, and about a ±10% variation in the signal acceptance.

Observed and expected 95% CL exclusion limits are set on M_D as a function of n using the CL_s approach, for which a simultaneous fit to the signal and control regions in the exclusive $E_{\mathrm{T}}^{\mathrm{miss}}$ bins is performed, including statistical and systematic uncertainties. Uncertainties in the signal acceptance times efficiency, the background predictions, and the luminosity are considered, and correlations between systematic uncertainties in signal and background predictions are taken into account. The fit accounts for the contamination of the control regions by signal events which a priori is estimated to be very small. In addition, observed limits are computed using $\pm 1\sigma$ variations of the theoretical predictions for the ADD cross sections. The -1σ variations of the ADD theoretical cross sections result in about a 6% decrease in the nominal observed limits. Figure 4 and Table 10 present the results in the case of the ADD model. Values of M_D below 6.58 TeV at $n = 2$ and below 4.31 TeV at $n = 6$ are excluded at 95% CL, which extend the exclusion from previous results using 8 TeV data [37].

As discussed in Refs. [5, 37], the analysis partially probes the phase-space region with $\hat{s} > M_D^2$, where $\sqrt{\hat{s}}$ is the center-of-mass energy of the hard interaction. This challenges the validity of model implementation and the lower bounds on M_D, as they depend on the unknown ultraviolet behavior of the effective theory. The observed 95% CL limits are recomputed after suppressing, with a weighting factor $M_D^4/\hat{s}^2$, the signal events with $\hat{s} > M_D^2$, here referred to as damping. This results in a decrease of the quoted 95% CL lower limit on M_D which is negligible for $n = 2$ and about 5% for $n = 6$.

Table 10: The 95% CL observed and expected lower limits on the fundamental Planck scale in $4 + n$ dimensions, M_D, as a function of the number of extra dimensions n, considering nominal LO signal cross sections. The impact of the $\pm 1\sigma$ theoretical uncertainty on the observed limits and the expected $\pm 1\sigma$ range of limits in the absence of a signal are also given. Finally, the 95% CL observed limits after damping of the signal cross section for $\hat{s} > M_D^2$ (see text) are quoted in parentheses.

95% CL lower limits on M_D [TeV]				
n extra	95% CL observed limit		95% CL expected limit	
dimensions	Nominal (Nominal after damping)	$\pm 1\sigma$ (theory)	Nominal	$\pm 1\sigma$ (expected)
2	6.58 (6.58)	$^{+0.52}_{-0.42}$	6.88	$^{+0.65}_{-0.64}$
3	5.46 (5.44)	$^{+0.45}_{-0.34}$	5.67	$^{+0.41}_{-0.41}$
4	4.81 (4.74)	$^{+0.41}_{-0.29}$	4.96	$^{+0.29}_{-0.29}$
5	4.48 (4.34)	$^{+0.41}_{-0.26}$	4.60	$^{+0.23}_{-0.23}$
6	4.31 (4.10)	$^{+0.41}_{-0.24}$	4.38	$^{+0.19}_{-0.19}$

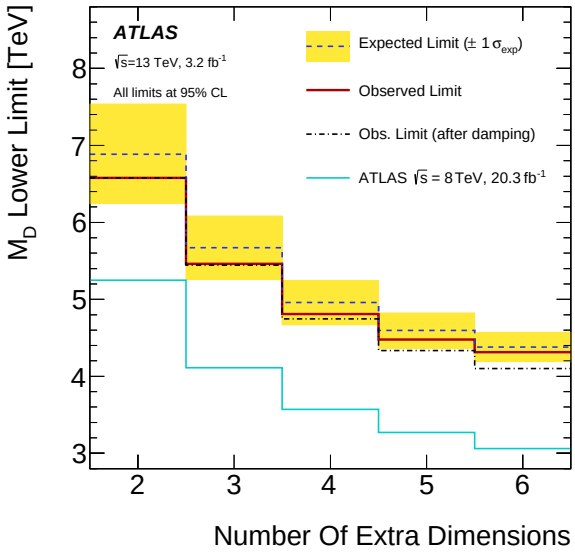

Figure 4: Observed and expected 95% CL lower limits on the fundamental Planck scale in $4+n$ dimensions, M_D, as a function of the number of extra dimensions. The shaded area around the expected limit indicates the expected $\pm 1\sigma$ range of limits in the absence of a signal. Finally, the thin dashed line shows the 95% CL observed limits after the suppression of the events with $\hat{s} > M_D^2$ (damping) is applied, as described in the text. The results from this analysis are compared to previous results from the ATLAS Collaboration at $\sqrt{s} = 8$ TeV [37].

8.2 Squark pair production

The results are translated into exclusion limits computed separately for stop pair production with $\tilde{t}_1 \to c + \tilde{\chi}_1^0$, squark pair production with $\tilde{q} \to q + \tilde{\chi}_1^0$ ($q = u, d, c, s$), and sbottom pair production with $\tilde{b}_1 \to b + \tilde{\chi}_1^0$, as a function of the squark mass for different neutralino masses. As an example, in the case of stop pair production the typical $A \times \epsilon$ of the selection criteria varies, with increasing stop and neutralino masses, between 0.7% and 1.4% for IM1 and between 0.06% and 0.8% for IM7. Observed and expected 95% CL exclusion limits are calculated using a simultaneous fit to the signal and control regions in exclusive $E_{\mathrm{T}}^{\mathrm{miss}}$ bins, as in the case of the ADD models.

The systematic uncertainties in the SUSY signal yields are also determined following a procedure close to that for the ADD case. The uncertainties related to the jet and $E_{\mathrm{T}}^{\mathrm{miss}}$ scales and resolutions introduce uncertainties in the signal yields which vary between ±0.2% and ±7% for different selections and squark and neutralino masses. In addition, the uncertainty in the integrated luminosity is included. The uncertainties related to the modeling of initial- and final-state gluon radiation translate into a ±7% to ±17% uncertainty in the signal yields. The uncertainties due to the PDFs result in a ±5% to ±17% uncertainty in the signal yields. Finally, the variations of the renormalization and factorization scales introduce a ±4% to ±13% uncertainty in the signal yields.

Figure 5 presents the results in the case of the $\tilde{t}_1 \to c + \tilde{\chi}_1^0$ signal. The previous limits from the ATLAS Collaboration [10] are also shown. As anticipated, the monojet-like selection improves significantly the sensitivity at very low Δm. In the compressed scenario with the stop and neutralino nearly degenerate in mass, the exclusion extends up to stop masses of 323 GeV. The region with $\Delta m < 5$ GeV is not considered in the exclusion since in this regime the stop could become long-lived. Figure 6 (left) presents

the observed and expected 95% CL exclusion limits as a function of the sbottom mass and the sbottom–neutralino mass difference for the $\tilde{b}_1 \to b + \tilde{\chi}_1^0$ decay channel. In the scenario with $m_{\tilde{b}_1} - m_{\tilde{\chi}_1^0} \sim m_b$, this analysis extends the 95% CL exclusion limits up to a sbottom mass of 323 GeV. Similarly, Fig. 6 (right) presents the observed and expected 95% CL exclusion limits as a function of the squark mass and the squark–neutralino mass difference for $\tilde{q} \to q + \tilde{\chi}_1^0$ ($q = u, d, c, s$). In the compressed scenario with similar squark and neutralino masses, squark masses below 608 GeV are excluded at 95% CL. These results significantly extend previous exclusion limits [10, 93, 94].

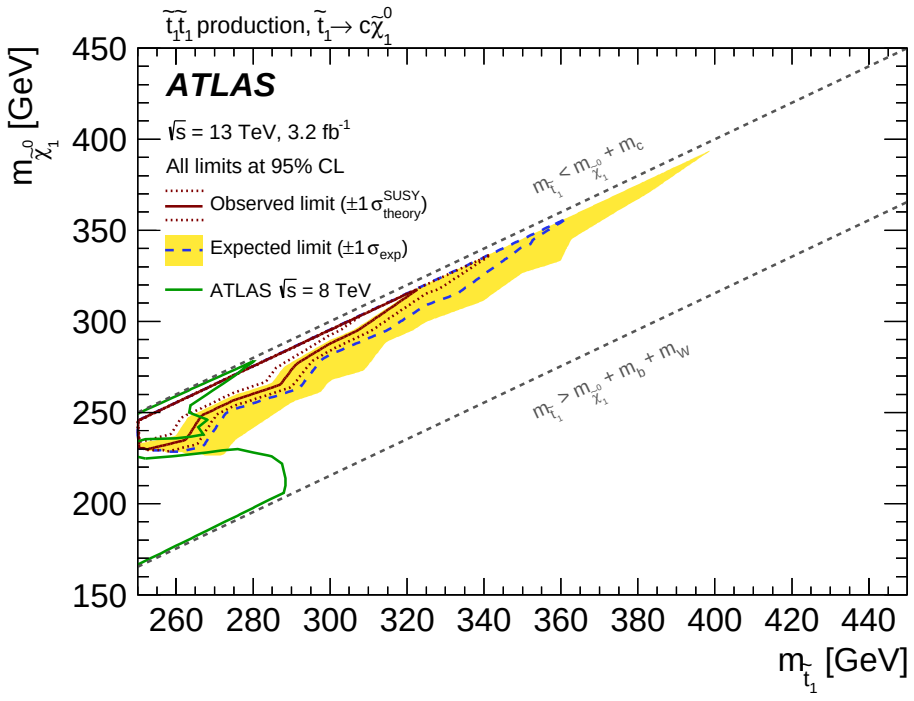

Figure 5: Excluded region at the 95% CL in the $(\tilde{t}_1, \tilde{\chi}_1^0)$ mass plane for the decay channel $\tilde{t}_1 \to c + \tilde{\chi}_1^0$ (BR = 100%). The dotted lines around the observed limit indicate the range of observed limits corresponding to $\pm 1\sigma$ variations of the NLO SUSY cross-section predictions. The shaded area around the expected limit indicates the expected $\pm 1\sigma$ ranges of limits in the absence of a signal. The results from this analysis are compared to previous results from the ATLAS Collaboration at $\sqrt{s} = 8$ TeV [10].

8.3 Weakly interacting massive particles

The results are translated into exclusion limits on the WIMP pair-production, assuming the exchange of an axial-vector mediator in the s-channel. For on-shell WIMP pair-production, where $m_A > 2m_\chi$, typical $A \times \epsilon$ values for the signal models with a 1 TeV mediator range from 25% to 2% for IM1 and IM7 selections, respectively.

The effect of experimental uncertainties related to jet and $E_{\mathrm{T}}^{\mathrm{miss}}$ scales and resolutions is found to be similar to the effect in the ADD model. The uncertainty related to the modeling of the initial- and final-state radiation translates into ±20% uncertainty in the acceptance and is neglected for the cross section. The choice of different PDF sets results in up to ±20% uncertainty in the acceptance and ±10% uncertainty in the cross section. Varying the renormalization and factorization scales introduces ±5% variations of

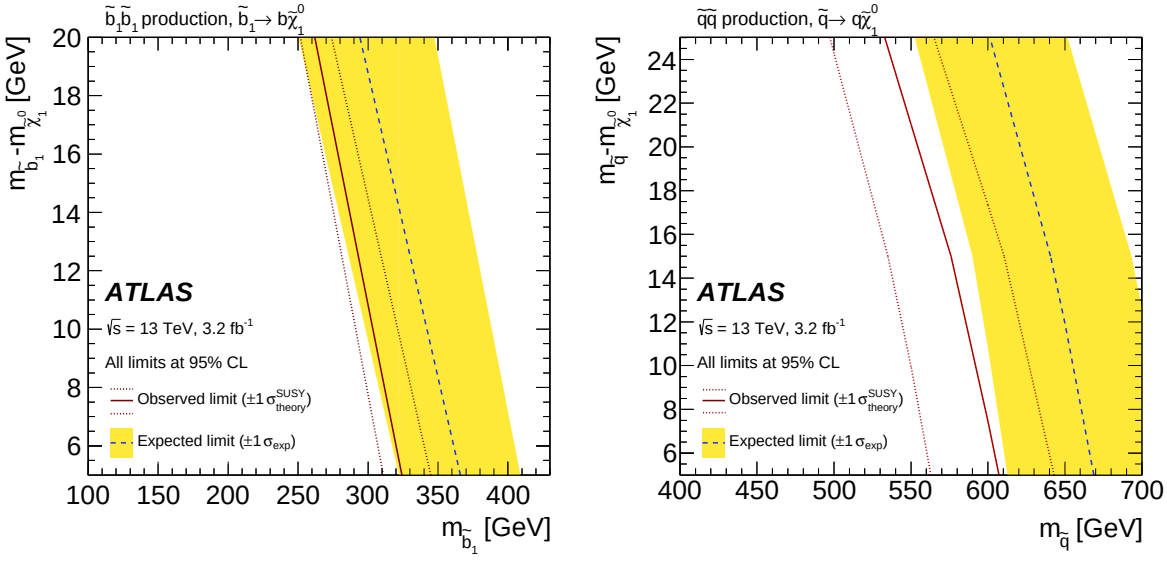

Figure 6: Exclusion region at 95% CL as a function of squark mass and the squark–neutralino mass difference for (left) the decay channel $\tilde{b}_1 \to b+\tilde{\chi}_1^0$ and (right) $\tilde{q} \to q+\tilde{\chi}_1^0$ ($q = u, d, c, s$). The dotted lines around the observed limit indicate the range of observed limits corresponding to $\pm 1\sigma$ variations of the NLO SUSY cross-section predictions. The shaded area around the expected limit indicates the expected $\pm 1\sigma$ ranges of limits in the absence of a signal.

the cross section and a ±3% change in the acceptance. In addition, the uncertainty in the integrated luminosity is included.

Figure 7 (left) shows the observed and expected 95% CL exclusion limits in the m_χ–m_A parameter plane for a simplified model with an axial-vector mediator, Dirac WIMPs, and couplings $g_q = 1/4$ and $g_\chi = 1$. A minimal mediator width is assumed. In addition, observed limits are shown using $\pm 1\sigma$ theoretical uncertainties in the signal cross sections. In the on-shell regime, the models with mediator masses up to 1 TeV are excluded. This analysis loses sensitivity to the models in the off-shell regime, where the decay into a pair of WIMPs is kinematically suppressed. The perturbative unitarity is violated in the parameter region defined by $m_\chi > \sqrt{\pi/2}\, m_A$ [95]. The masses corresponding to the correct relic density as measured by the Planck and WMAP satellites [35, 36], in the absence of any interaction other than the one considered, are indicated in the figure as a line that crosses the excluded region at $m_A \sim 880$ GeV and $m_\chi \sim 270$ GeV. The region towards lower WIMP masses or higher mediator masses corresponds to dark matter overproduction. On the opposite side of the curve, other WIMP production mechanisms need to exist in order to explain the observed dark matter relic density.

In Fig. 7 (right) the results are translated into 90% CL exclusion limits on the spin-dependent WIMP–proton scattering cross section as a function of the WIMP mass, following the prescriptions explained in Refs. [41, 42], and are compared to results from the direct-detection experiments XENON100 [96], LUX [97], and PICO [98, 99]. This comparison is model-dependent and solely valid in the context of this particular Z'-like model. In this case, stringent limits on the scattering cross section of the order of 10^{-42} cm^2 up to WIMP masses of about 300 GeV are inferred from this analysis, and complement the results from direct-detection experiments for $m_\chi < 10$ GeV. The loss of sensitivity in models where WIMPs are produced off-shell is expressed by the turn of the exclusion line, reaching back to low WIMP masses and intercepting the exclusion lines from the direct-detection experiments at around $m_\chi = 80$ GeV.

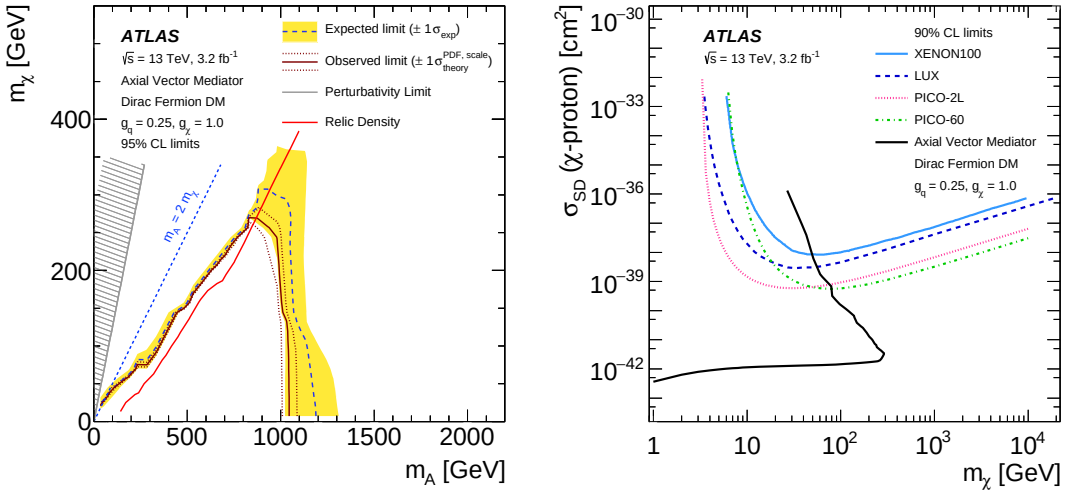

Figure 7: Left: 95% CL exclusion contours in the m_χ–m_A parameter plane. The solid (dashed) curve shows the median of the observed (expected) limit, while the bands indicate the $\pm 1\sigma$ theory uncertainties in the observed limit and $\pm 1\sigma$ range of the expected limit in the absence of a signal. The red curve corresponds to the expected relic density. The region excluded due to perturbativity, defined by $m_\chi > \sqrt{\pi/2}\, m_A$, is indicated by the hatched area. Right: A comparison of the inferred limits to the constraints from direct detection experiments on the spin-dependent WIMP–proton scattering cross section in the context of the Z'-like simplified model with axial-vector couplings. Unlike in the m_χ–m_A parameter plane, the limits are shown at 90% CL. The results from this analysis, excluding the region to the left of the contour, are compared with limits from the XENON100 [96], LUX [97], and PICO [98, 99] experiments. The comparison is model-dependent and solely valid in the context of this model, assuming minimal mediator width and the coupling values $g_q = 1/4$ and $g_\chi = 1$.

9 Conclusions

In summary, results are reported from a search for new phenomena in events with an energetic jet and large missing transverse momentum in proton–proton collisions at $\sqrt{s} = 13$ TeV at the LHC, based on data corresponding to an integrated luminosity of $3.2\,\text{fb}^{-1}$ collected by the ATLAS experiment in 2015. The measurements are in agreement with the SM predictions.

The results are translated into model-independent 95% confidence-level upper limits on $\sigma \times A \times \epsilon$ in the range 553–19 fb, depending on the selection criteria considered. The results are presented in terms of lower limits on the fundamental Planck scale, M_D, versus the number of extra spatial dimensions in the ADD LED model. Values of M_D below 6.58 TeV at $n = 2$ and below 4.31 TeV at $n = 6$ are excluded at 95% CL. Similarly, the results are interpreted in terms of the search for squark pair production in a compressed supersymmetric scenario. In the case of stop and sbottom pair production with $\tilde{t}_1 \to c + \tilde{\chi}_1^0$ and $\tilde{b}_1 \to b + \tilde{\chi}_1^0$, respectively, squark masses below 323 GeV are excluded at 95% CL. In the case of squark pair production with $\tilde{q} \to q + \tilde{\chi}_1^0$ ($q = u, d, c, s$) squark masses below 608 GeV are excluded. Altogether, these results extend the exclusion from previous analyses at the LHC.

Finally, the results are interpreted in terms of upper limits on the pair-production cross section of WIMPs. A simplified model is used with an axial-vector mediator, given couplings to fermions $g_\chi = 1$ and $g_q = 1/4$, and considering Dirac fermions as dark matter candidates. Mediator masses below 1 TeV are excluded at 95% CL for WIMP masses below 250 GeV. These results are translated, in a model-dependent manner, into upper limits on spin-dependent contributions to the WIMP–nucleon elastic cross

section as a function of the WIMP mass. WIMP–proton cross sections above 10^{-42} cm^2 are excluded at 90% CL for WIMP masses below 10 GeV, complementing results from direct-detection experiments.

Acknowledgments

We thank CERN for the very successful operation of the LHC, as well as the support staff from our institutions without whom ATLAS could not be operated efficiently.

We acknowledge the support of ANPCyT, Argentina; YerPhI, Armenia; ARC, Australia; BMWFW and FWF, Austria; ANAS, Azerbaijan; SSTC, Belarus; CNPq and FAPESP, Brazil; NSERC, NRC and CFI, Canada; CERN; CONICYT, Chile; CAS, MOST and NSFC, China; COLCIENCIAS, Colombia; MSMT CR, MPO CR and VSC CR, Czech Republic; DNRF and DNSRC, Denmark; IN2P3-CNRS, CEA-DSM/IRFU, France; GNSF, Georgia; BMBF, HGF, and MPG, Germany; GSRT, Greece; RGC, Hong Kong SAR, China; ISF, I-CORE and Benoziyo Center, Israel; INFN, Italy; MEXT and JSPS, Japan; CNRST, Morocco; FOM and NWO, Netherlands; RCN, Norway; MNiSW and NCN, Poland; FCT, Portugal; MNE/IFA, Romania; MES of Russia and NRC KI, Russian Federation; JINR; MESTD, Serbia; MSSR, Slovakia; ARRS and MIZŠ, Slovenia; DST/NRF, South Africa; MINECO, Spain; SRC and Wallenberg Foundation, Sweden; SERI, SNSF and Cantons of Bern and Geneva, Switzerland; MOST, Taiwan; TAEK, Turkey; STFC, United Kingdom; DOE and NSF, United States of America. In addition, individual groups and members have received support from BCKDF, the Canada Council, CANARIE, CRC, Compute Canada, FQRNT, and the Ontario Innovation Trust, Canada; EPLANET, ERC, FP7, Horizon 2020 and Marie Skłodowska-Curie Actions, European Union; Investissements d'Avenir Labex and Idex, ANR, Région Auvergne and Fondation Partager le Savoir, France; DFG and AvH Foundation, Germany; Herakleitos, Thales and Aristeia programmes co-financed by EU-ESF and the Greek NSRF; BSF, GIF and Minerva, Israel; BRF, Norway; Generalitat de Catalunya, Generalitat Valenciana, Spain; the Royal Society and Leverhulme Trust, United Kingdom.

The crucial computing support from all WLCG partners is acknowledged gratefully, in particular from CERN and the ATLAS Tier-1 facilities at TRIUMF (Canada), NDGF (Denmark, Norway, Sweden), CC-IN2P3 (France), KIT/GridKA (Germany), INFN-CNAF (Italy), NL-T1 (Netherlands), PIC (Spain), ASGC (Taiwan), RAL (UK) and BNL (USA) and in the Tier-2 facilities worldwide.

References

[1] CMS Collaboration, *Search for New Physics with a Mono-Jet and Missing Transverse Energy in pp Collisions at* $\sqrt{s} = 7$ *TeV*, Phys. Rev. Lett. **107** (2011) 201804.

[2] CMS Collaboration, *Search for dark matter and large extra dimensions in monojet events in pp collisions at* $\sqrt{s} = 7$ *TeV*, JHEP **09** (2012) 094.

[3] CMS Collaboration, *Search for Dark Matter and Large Extra Dimensions in pp Collisions Yielding a Photon and Missing Transverse Energy*, Phys. Rev. Lett. **108** (2012) 261803.

[4] ATLAS Collaboration, *Search for new phenomena with the monojet and missing transverse momentum signature using the ATLAS detector in* $\sqrt{s} = 7$ *TeV proton-proton collisions*, Phys. Lett. B **705** (2011) 294.

[5] ATLAS Collaboration, *Search for dark matter candidates and large extra dimensions in events with a jet and missing transverse momentum with the ATLAS detector*, JHEP **04** (2013) 075.

[6] ATLAS Collaboration, *Search for dark matter candidates and large extra dimensions in events with a photon and missing transverse momentum in pp collision data at $\sqrt{s} = 7$ TeV with the ATLAS detector*, Phys. Rev. Lett. **110** (2013) 011802.

[7] CMS Collaboration, *Search for dark matter, extra dimensions, and unparticles in monojet events in proton–proton collisions at $\sqrt{s} = 8$ TeV*, Eur. Phys. J. C **75** (2015) 235.

[8] CMS Collaboration, *Search for new phenomena in monophoton final states in proton-proton collisions at $\sqrt{s} = 8$ TeV*, Phys. Lett. B **755** (2016) 102.

[9] CDF Collaboration, T. Affolder et al., *Limits on gravitino production and new processes with large missing transverse energy in $p\bar{p}$ collisions at $\sqrt{s} = 1.8$ TeV*, Phys. Rev. Lett. **85** (2000) 1378.

[10] ATLAS Collaboration, *Search for pair-produced third-generation squarks decaying via charm quarks or in compressed supersymmetric scenarios in pp collisions at $\sqrt{s} = 8$ TeV with the ATLAS detector*, Phys. Rev. D **90** (2014) 052008.

[11] ATLAS Collaboration, *Search for dark matter in events with heavy quarks and missing transverse momentum in pp collisions with the ATLAS detector*, Eur. Phys. J. C **75** (2015) 92.

[12] ATLAS Collaboration, *Search for dark matter in events with a Z boson and missing transverse momentum in pp collisions at $\sqrt{s}$=8 TeV with the ATLAS detector*, Phys. Rev. D **90** (2014) 012004.

[13] ATLAS Collaboration, *Search for dark matter in events with a hadronically decaying W or Z boson and missing transverse momentum in pp collisions at $\sqrt{s} = 8$ TeV with the ATLAS detector*, Phys. Rev. Lett. **112** (2014) 041802.

[14] CMS Collaboration, *Search for physics beyond the standard model in final states with a lepton and missing transverse energy in proton-proton collisions at $\sqrt{s} = 8$ TeV*, Phys. Rev. D **91** (2015) 092005.

[15] CMS Collaboration, *Searches for third-generation squark production in fully hadronic final states in proton-proton collisions at $\sqrt{s} = 8$ TeV*, JHEP **06** (2015) 116.

[16] N. Arkani-Hamed, S. Dimopoulos, and G. Dvali, *The Hierarchy problem and new dimensions at a millimeter*, Phys. Lett. B **429** (1998) 263.

[17] H. Miyazawa, *Baryon Number Changing Currents*, Prog. Theor. Phys. **36 (6)** (1966) 1266.

[18] P. Ramond, *Dual Theory for Free Fermions*, Phys. Rev. D **3** (1971) 2415.

[19] Y. A. Golfand and E. P. Likhtman, *Extension of the Algebra of Poincare Group Generators and Violation of p Invariance*, JETP Lett. **13** (1971) 323.

[20] A. Neveu and J. H. Schwarz, *Factorizable dual model of pions*, Nucl. Phys. B **31** (1971) 86.

[21] A. Neveu and J. H. Schwarz, *Quark Model of Dual Pions*, Phys. Rev. D **4** (1971) 1109.

[22] J. Gervais and B. Sakita, *Field theory interpretation of supergauges in dual models*, Nucl. Phys. B **34** (1971) 632.

[23] D. V. Volkov and V. P. Akulov, *Is the Neutrino a Goldstone Particle?* Phys. Lett. B **46** (1973) 109.

[24] J. Wess and B. Zumino, *A Lagrangian Model Invariant Under Supergauge Transformations*, Phys. Lett. B **49** (1974) 52.

[25] J. Wess and B. Zumino, *Supergauge Transformations in Four-Dimensions*, Nucl. Phys. B **70** (1974) 39.

[26] R. Barbieri and G. Giudice, *Upper Bounds on Supersymmetric Particle Masses*, Nucl. Phys. B **306** (1988) 63.

[27] P. Fayet, *Supersymmetry and Weak, Electromagnetic and Strong Interactions*, Phys. Lett. B **64** (1976) 159.

[28] P. Fayet, *Spontaneously Broken Supersymmetric Theories of Weak, Electromagnetic and Strong Interactions*, Phys. Lett. B **69** (1977) 489.

[29] G. R. Farrar and P. Fayet, *Phenomenology of the Production, Decay, and Detection of New Hadronic States Associated with Supersymmetry*, Phys. Lett. B **76** (1978) 575.

[30] P. Fayet, *Relations Between the Masses of the Superpartners of Leptons and Quarks, the Goldstino Couplings and the Neutral Currents*, Phys. Lett. B **84** (1979) 416.

[31] S. Dimopoulos and H. Georgi, *Softly Broken Supersymmetry and SU(5)*, Nucl. Phys. B **193** (1981) 150.

[32] G. Bertone, D. Hooper, and J. Silk, *Particle dark matter: Evidence, candidates and constraints*, Phys. Rept. **405** (2005) 279.

[33] G. Steigman and M. S. Turner, *Cosmological Constraints on the Properties of Weakly Interacting Massive Particles*, Nucl. Phys. B **253** (1985) 375.

[34] E. W. Kolb and M. S. Turner, *The Early universe*, Front. Phys. **69** (1990) 1.

[35] Planck Collaboration, R. Adam et al., *Planck 2015 results. I. Overview of products and scientific results*, (2015), arXiv:1502.01582 [astro-ph.CO].

[36] G. Hinshaw et al., *Nine-year Wilkinson Microwave Anisotropy Probe (WMAP) Observations: Cosmological Parameter Results*, Astrophys. J. Suppl. Ser. **208** (2013) 19.

[37] ATLAS Collaboration, *Search for new phenomena in final states with an energetic jet and large missing transverse momentum in pp collisions at* $\sqrt{s}$ *=8 TeV with the ATLAS detector*, Eur. Phys. J. C **75** (2015) 299, [Erratum: Eur. Phys. J.C 75,no.9,408(2015)].

[38] J. Goodman et al., *Constraints on Dark Matter from Colliders*, Phys. Rev. D **82** (2010) 116010.

[39] J. Abdallah et al., *Simplified Models for Dark Matter Searches at the LHC*, Phys. Dark Univ. **9-10** (2015) 8.

[40] D. Abercrombie et al., *Dark matter benchmark models for early LHC Run-2 searches: report of the ATLAS/CMS Dark Matter Forum*, (2015), arXiv:1507.00966 [hep-ex].

[41] O. Buchmueller et al., *Characterising dark matter searches at colliders and direct detection experiments: Vector mediators*, JHEP **01** (2015) 037.

[42] G. Busoni et al., *Recommendations on presenting LHC searches for missing transverse energy signals using simplified s-channel models of dark matter*, (2016), ed. by A. Boveia et al., arXiv:1603.04156 [hep-ex].

[43] G. Busoni et al., *On the Validity of the Effective Field Theory for Dark Matter Searches at the LHC*, Phys. Lett. B **728** (2014) 412.

[44] ATLAS Collaboration, *The ATLAS Experiment at the CERN Large Hadron Collider*, JINST **3** (2008) S08003.

[45] ATLAS Collaboration, "ATLAS Insertable B-Layer Technical Design Report," tech. rep. CERN-LHCC-2010-013. ATLAS-TDR-19, CERN, 2010, URL: http://cds.cern.ch/record/1291633.

[46] ATLAS Collaboration, *2015 start-up trigger menu and initial performance assessment of the ATLAS trigger using Run-2 data*, ATL-DAQ-PUB-2016-001, 2016, URL: http://cds.cern.ch/record/2136007.

[47] T. Gleisberg et al., *Event generation with SHERPA 1.1*, JHEP **02** (2009) 007.

[48] T. Gleisberg and S. Höche, *Comix, a new matrix element generator*, JHEP **12** (2008) 039.

[49] F. Cascioli, P. Maierhofer, and S. Pozzorini, *Scattering Amplitudes with Open Loops*, Phys. Rev. Lett. **108** (2012) 111601.

[50] S. Schumann and F. Krauss, *A Parton shower algorithm based on Catani-Seymour dipole factorisation*, JHEP **03** (2008) 038.

[51] S. Höche et al., *QCD matrix elements + parton showers: The NLO case*, JHEP **04** (2013) 027.

[52] H.-L. Lai et al., *New parton distributions for collider physics*, Phys. Rev. D **82** (2010) 074024.

[53] S. Catani et al., *Vector boson production at hadron colliders: a fully exclusive QCD calculation at NNLO*, Phys. Rev. Lett. **103** (2009) 082001.

[54] S. Catani and M. Grazzini, *An NNLO subtraction formalism in hadron collisions and its application to Higgs boson production at the LHC*, Phys. Rev. Lett. **98** (2007) 222002.

[55] A. D. Martin et al., *Parton distributions for the LHC*, Eur. Phys. J. C **63** (2009) 189.

[56] S. Frixione, P. Nason, and G. Ridolfi, *A Positive-Weight Next-to-Leading-Order Monte Carlo for Heavy Flavour Hadroproduction*, JHEP **09** (2007) 126.

[57] T. Sjöstrand, S. Mrenna, and P. Z. Skands, *PYTHIA 6.4 Physics and Manual*, JHEP **05** (2006) 026.

[58] J. Pumplin et al., *New generation of parton distributions with uncertainties from global QCD analysis*, JHEP **07** (2002) 012.

[59] P. Z. Skands, *Tuning Monte Carlo Generators: The Perugia Tunes*, Phys. Rev. D **82** (2010) 074018.

[60] D. J. Lange, *The EvtGen particle decay simulation package*, Nucl. Instrum. Meth. A **462** (2001) 152.

[61] J. M. Campbell, R. K. Ellis, and C. Williams, *Vector boson pair production at the LHC*, JHEP **07** (2011) 018.

[62] R. D. Ball et al., *Parton distributions with LHC data*, Nucl. Phys. B **867** (2013) 244.

[63] J. Alwall et al., *The automated computation of tree-level and next-to-leading order differential cross sections, and their matching to parton shower simulations*, JHEP **07** (2014) 079.

[64] ATLAS Collaboration, *ATLAS Run 1 Pythia8 tunes*, ATL-PHYS-PUB-2014-021, 2014, URL: http://cds.cern.ch/record/1966419.

[65] L. Lönnblad and S. Prestel, *Matching Tree-Level Matrix Elements with Interleaved Showers*, JHEP **03** (2012) 019.

[66] W. Beenakker et al., *Stop production at hadron colliders*, Nucl. Phys. B **515** (1998) 3.

[67] W. Beenakker et al., *Supersymmetric top and bottom squark production at hadron colliders*, JHEP. **08** (2010) 098.

[68] W. Beenakker et al., *Squark and gluino hadroproduction*, Int. J. Mod. Phys. A **26** (2011) 2637.

[69] C. Borschensky et al., *Squark and gluino production cross sections in pp collisions at* $\sqrt{s}$ *= 13, 14, 33 and 100 TeV*, Eur. Phys. J. C **74** (2014) 3174.

[70] S. Alioli et al., *A general framework for implementing NLO calculations in shower Monte Carlo programs: the POWHEG BOX*, JHEP **06** (2010) 043.

[71] S. Frixione, P. Nason, and C. Oleari, *Matching NLO QCD computations with Parton Shower simulations: the POWHEG method*, JHEP **11** (2007) 070.

[72] P. Nason, *A New method for combining NLO QCD with shower Monte Carlo algorithms*, JHEP **11** (2004) 040.

[73] U. Haisch, F. Kahlhöfer, and E. Re, *QCD effects in mono-jet searches for dark matter*, JHEP **12** (2013) 007.

[74] R. D. Ball et al., *Parton distributions for the LHC Run II*, JHEP **04** (2015) 040.

[75] ATLAS Collaboration, *The ATLAS Simulation Infrastructure*, Eur. Phys. J. C **70** (2010) 823.

[76] S. Agostinelli et al., *GEANT4: A Simulation toolkit*, Nucl. Instrum. Meth. A **506** (2003) 250.

[77] M. Cacciari, G. P. Salam, and G. Soyez, *The anti-k_t jet clustering algorithm*, JHEP **04** (2008) 063.

[78] ATLAS Collaboration, *Jet energy measurement with the ATLAS detector in proton-proton collisions at $\sqrt{s}$ = 7 TeV*, Eur. Phys. J. C **73** (2013) 2304.

[79] ATLAS Collaboration, *Tagging and suppression of pileup jets with the ATLAS detector*, ATLAS-CONF-2014-018, 2014, URL: http://cds.cern.ch/record/1700870.

[80] ATLAS Collaboration, *Muon reconstruction performance of the ATLAS detector in proton–proton collision data at $\sqrt{s}$=13 TeV*, (2016), arXiv:1603.05598 [hep-ex].

[81] ATLAS Collaboration, *Electron efficiency measurements with the ATLAS detector using the 2012 LHC proton–proton collision data*, ATLAS-CONF-2014-032, 2014, URL: http://cdsweb.cern.ch/record/1706245.

[82] ATLAS Collaboration, *Performance of Missing Transverse Momentum Reconstruction in Proton-Proton Collisions at 7 TeV with ATLAS*, Eur. Phys. J. C **72** (2012) 1844.

[83] ATLAS Collaboration, *Selection of jets produced in 13 TeV proton-proton collisions with the ATLAS detector*, ATLAS-CONF-2015-029, 2015, URL: http://cds.cern.ch/record/2037702.

[84] ATLAS Collaboration, *Characterisation and mitigation of beam-induced backgrounds observed in the ATLAS detector during the 2011 proton-proton run*, JINST **8** (2013) P07004.

[85] ATLAS Collaboration, *Search for squarks and gluinos with the ATLAS detector in final states with jets and missing transverse momentum using 4.7 fb^{-1} of $\sqrt{s}$ = 7 TeV proton-proton collision data*, Phys. Rev. D **87** (2013) 012008.

[86] G. Cowan et al., *Asymptotic formulae for likelihood-based tests of new physics*, Eur. Phys. J. C **71** (2011) 1554.

[87] A. Denner et al., *Electroweak corrections to monojet production at the LHC*, Eur. Phys. J. C **73** (2013) 2297.

[88] A. Denner et al., *Electroweak corrections to dilepton + jet production at hadron colliders*, JHEP **06** (2011) 069.

[89] A. Denner et al., *Electroweak corrections to W + jet hadroproduction including leptonic W-boson decays*, JHEP **08** (2009) 075.

[90] ATLAS Collaboration, *Improved luminosity determination in pp collisions at $\sqrt{s}$ = 7 TeV using the ATLAS detector at the LHC*, Eur. Phys. J. C **73** (2013) 2518.

[91] L. A. Harland-Lang et al., *Parton distributions in the LHC era: MMHT 2014 PDFs*, Eur. Phys. J. C **75** (2015) 204.

[92] A. L. Read, *Presentation of search results: The CL_s technique*, J. Phys. G **28** (2002) 2693–2704.

[93] CDF Collaboration, T. Aaltonen et al., *Search for Scalar Top Quark Production in $p\bar{p}$ Collisions at $\sqrt{s} = 1.96$ TeV*, JHEP **10** (2012) 158.

[94] D0 Collaboration, V.M Abazov et al., *Search for scalar top quarks in the acoplanar charm jets and missing transverse energy final state in $p\bar{p}$ collisions at $\sqrt{s} = 1.96$ TeV*, Phys. Lett. B **665** (2008) 1.

[95] F. Kahlhöfer et al., *Implications of unitarity and gauge invariance for simplified dark matter models*, JHEP **02** (2016) 016.

[96] XENON100 Collaboration, E. Aprile et al., *Limits on spin-dependent WIMP-nucleon cross sections from 225 live days of XENON100 data*, Phys. Rev. Lett. **111** (2013) 021301.

[97] LUX Collaboration, D. S. Akerib et al., *First spin-dependent WIMP-nucleon cross section limits from the LUX experiment*, (2016), arXiv:1602.03489 [hep-ex].

[98] C. Amole et al., *Dark matter search results from the PICO-60 CF_3I bubble chamber*, Phys. Rev. D **93** (2016) 052014.

[99] PICO Collaboration, C. Amole et al., *Improved Dark Matter Search Results from PICO-2L Run-2*, Submitted to: Phys. Rev. D (2016), arXiv:1601.03729 [astro-ph.CO].

The ATLAS Collaboration

M. Aaboud[136d], G. Aad[87], B. Abbott[114], J. Abdallah[65], O. Abdinov[12], B. Abeloos[118], R. Aben[108], O.S. AbouZeid[138], N.L. Abraham[150], H. Abramowicz[154], H. Abreu[153], R. Abreu[117], Y. Abulaiti[147a,147b], B.S. Acharya[164a,164b,a], L. Adamczyk[40a], D.L. Adams[27], J. Adelman[109], S. Adomeit[101], T. Adye[132], A.A. Affolder[76], T. Agatonovic-Jovin[14], J. Agricola[56], J.A. Aguilar-Saavedra[127a,127f], S.P. Ahlen[24], F. Ahmadov[67,b], G. Aielli[134a,134b], H. Akerstedt[147a,147b], T.P.A. Åkesson[83], A.V. Akimov[97], G.L. Alberghi[22a,22b], J. Albert[169], S. Albrand[57], M.J. Alconada Verzini[73], M. Aleksa[32], I.N. Aleksandrov[67], C. Alexa[28b], G. Alexander[154], T. Alexopoulos[10], M. Alhroob[114], M. Aliev[75a,75b], G. Alimonti[93a], J. Alison[33], S.P. Alkire[37], B.M.M. Allbrooke[150], B.W. Allen[117], P.P. Allport[19], A. Aloisio[105a,105b], A. Alonso[38], F. Alonso[73], C. Alpigiani[139], M. Alstaty[87], B. Alvarez Gonzalez[32], D. Álvarez Piqueras[167], M.G. Alviggi[105a,105b], B.T. Amadio[16], K. Amako[68], Y. Amaral Coutinho[26a], C. Amelung[25], D. Amidei[91], S.P. Amor Dos Santos[127a,127c], A. Amorim[127a,127b], S. Amoroso[32], G. Amundsen[25], C. Anastopoulos[140], L.S. Ancu[51], N. Andari[109], T. Andeen[11], C.F. Anders[60b], G. Anders[32], J.K. Anders[76], K.J. Anderson[33], A. Andreazza[93a,93b], V. Andrei[60a], S. Angelidakis[9], I. Angelozzi[108], P. Anger[46], A. Angerami[37], F. Anghinolfi[32], A.V. Anisenkov[110,c], N. Anjos[13], A. Annovi[125a,125b], M. Antonelli[49], A. Antonov[99], F. Anulli[133a], M. Aoki[68], L. Aperio Bella[19], G. Arabidze[92], Y. Arai[68], J.P. Araque[127a], A.T.H. Arce[47], F.A. Arduh[73], J-F. Arguin[96], S. Argyropoulos[65], M. Arik[20a], A.J. Armbruster[144], L.J. Armitage[78], O. Arnaez[32], H. Arnold[50], M. Arratia[30], O. Arslan[23], A. Artamonov[98], G. Artoni[121], S. Artz[85], S. Asai[156], N. Asbah[44], A. Ashkenazi[154], B. Åsman[147a,147b], L. Asquith[150], K. Assamagan[27], R. Astalos[145a], M. Atkinson[166], N.B. Atlay[142], K. Augsten[129], G. Avolio[32], B. Axen[16], M.K. Ayoub[118], G. Azuelos[96,d], M.A. Baak[32], A.E. Baas[60a], M.J. Baca[19], H. Bachacou[137], K. Bachas[75a,75b], M. Backes[32], M. Backhaus[32], P. Bagiacchi[133a,133b], P. Bagnaia[133a,133b], Y. Bai[35a], J.T. Baines[132], O.K. Baker[176], E.M. Baldin[110,c], P. Balek[130], T. Balestri[149], F. Balli[137], W.K. Balunas[123], E. Banas[41], Sw. Banerjee[173,e], A.A.E. Bannoura[175], L. Barak[32], E.L. Barberio[90], D. Barberis[52a,52b], M. Barbero[87], T. Barillari[102], T. Barklow[144], N. Barlow[30], S.L. Barnes[86], B.M. Barnett[132], R.M. Barnett[16], Z. Barnovska[5], A. Baroncelli[135a], G. Barone[25], A.J. Barr[121], L. Barranco Navarro[167], F. Barreiro[84], J. Barreiro Guimarães da Costa[35a], R. Bartoldus[144], A.E. Barton[74], P. Bartos[145a], A. Basalaev[124], A. Bassalat[118], R.L. Bates[55], S.J. Batista[159], J.R. Batley[30], M. Battaglia[138], M. Bauce[133a,133b], F. Bauer[137], H.S. Bawa[144,f], J.B. Beacham[112], M.D. Beattie[74], T. Beau[82], P.H. Beauchemin[162], P. Bechtle[23], H.P. Beck[18,g], K. Becker[121], M. Becker[85], M. Beckingham[170], C. Becot[111], A.J. Beddall[20e], A. Beddall[20b], V.A. Bednyakov[67], M. Bedognetti[108], C.P. Bee[149], L.J. Beemster[108], T.A. Beermann[32], M. Begel[27], J.K. Behr[44], C. Belanger-Champagne[89], A.S. Bell[80], G. Bella[154], L. Bellagamba[22a], A. Bellerive[31], M. Bellomo[88], K. Belotskiy[99], O. Beltramello[32], N.L. Belyaev[99], O. Benary[154], D. Benchekroun[136a], M. Bender[101], K. Bendtz[147a,147b], N. Benekos[10], Y. Benhammou[154], E. Benhar Noccioli[176], J. Benitez[65], D.P. Benjamin[47], J.R. Bensinger[25], S. Bentvelsen[108], L. Beresford[121], M. Beretta[49], D. Berge[108], E. Bergeaas Kuutmann[165], N. Berger[5], J. Beringer[16], S. Berlendis[57], N.R. Bernard[88], C. Bernius[111], F.U. Bernlochner[23], T. Berry[79], P. Berta[130], C. Bertella[85], G. Bertoli[147a,147b], F. Bertolucci[125a,125b], I.A. Bertram[74], C. Bertsche[44], D. Bertsche[114], G.J. Besjes[38], O. Bessidskaia Bylund[147a,147b], M. Bessner[44], N. Besson[137], C. Betancourt[50], S. Bethke[102], A.J. Bevan[78], W. Bhimji[16], R.M. Bianchi[126], L. Bianchini[25], M. Bianco[32], O. Biebel[101], D. Biedermann[17], R. Bielski[86], N.V. Biesuz[125a,125b], M. Biglietti[135a], J. Bilbao De Mendizabal[51], H. Bilokon[49], M. Bindi[56], S. Binet[118], A. Bingul[20b], C. Bini[133a,133b], S. Biondi[22a,22b], D.M. Bjergaard[47], C.W. Black[151], J.E. Black[144], K.M. Black[24], D. Blackburn[139], R.E. Blair[6], J.-B. Blanchard[137], J.E. Blanco[79], T. Blazek[145a], I. Bloch[44], C. Blocker[25], W. Blum[85,*], U. Blumenschein[56], S. Blunier[34a],

G.J. Bobbink[108], V.S. Bobrovnikov[110,c], S.S. Bocchetta[83], A. Bocci[47], C. Bock[101], M. Boehler[50], D. Boerner[175], J.A. Bogaerts[32], D. Bogavac[14], A.G. Bogdanchikov[110], C. Bohm[147a], V. Boisvert[79], P. Bokan[14], T. Bold[40a], A.S. Boldyrev[164a,164c], M. Bomben[82], M. Bona[78], M. Boonekamp[137], A. Borisov[131], G. Borissov[74], J. Bortfeldt[101], D. Bortoletto[121], V. Bortolotto[62a,62b,62c], K. Bos[108], D. Boscherini[22a], M. Bosman[13], J.D. Bossio Sola[29], J. Boudreau[126], J. Bouffard[2], E.V. Bouhova-Thacker[74], D. Boumediene[36], C. Bourdarios[118], S.K. Boutle[55], A. Boveia[32], J. Boyd[32], I.R. Boyko[67], J. Bracinik[19], A. Brandt[8], G. Brandt[56], O. Brandt[60a], U. Bratzler[157], B. Brau[88], J.E. Brau[117], H.M. Braun[175,*], W.D. Breaden Madden[55], K. Brendlinger[123], A.J. Brennan[90], L. Brenner[108], R. Brenner[165], S. Bressler[172], T.M. Bristow[48], D. Britton[55], D. Britzger[44], F.M. Brochu[30], I. Brock[23], R. Brock[92], G. Brooijmans[37], T. Brooks[79], W.K. Brooks[34b], J. Brosamer[16], E. Brost[117], J.H Broughton[19], P.A. Bruckman de Renstrom[41], D. Bruncko[145b], R. Bruneliere[50], A. Bruni[22a], G. Bruni[22a], L.S. Bruni[108], BH Brunt[30], M. Bruschi[22a], N. Bruscino[23], P. Bryant[33], L. Bryngemark[83], T. Buanes[15], Q. Buat[143], P. Buchholz[142], A.G. Buckley[55], I.A. Budagov[67], F. Buehrer[50], M.K. Bugge[120], O. Bulekov[99], D. Bullock[8], H. Burckhart[32], S. Burdin[76], C.D. Burgard[50], B. Burghgrave[109], K. Burka[41], S. Burke[132], I. Burmeister[45], E. Busato[36], D. Büscher[50], V. Büscher[85], P. Bussey[55], J.M. Butler[24], C.M. Buttar[55], J.M. Butterworth[80], P. Butti[108], W. Buttinger[27], A. Buzatu[55], A.R. Buzykaev[110,c], S. Cabrera Urbán[167], D. Caforio[129], V.M. Cairo[39a,39b], O. Cakir[4a], N. Calace[51], P. Calafiura[16], A. Calandri[87], G. Calderini[82], P. Calfayan[101], L.P. Caloba[26a], D. Calvet[36], S. Calvet[36], T.P. Calvet[87], R. Camacho Toro[33], S. Camarda[32], P. Camarri[134a,134b], D. Cameron[120], R. Caminal Armadans[166], C. Camincher[57], S. Campana[32], M. Campanelli[80], A. Camplani[93a,93b], A. Campoverde[149], V. Canale[105a,105b], A. Canepa[160a], M. Cano Bret[35e], J. Cantero[115], R. Cantrill[127a], T. Cao[42], M.D.M. Capeans Garrido[32], I. Caprini[28b], M. Caprini[28b], M. Capua[39a,39b], R. Caputo[85], R.M. Carbone[37], R. Cardarelli[134a], F. Cardillo[50], I. Carli[130], T. Carli[32], G. Carlino[105a], L. Carminati[93a,93b], S. Caron[107], E. Carquin[34b], G.D. Carrillo-Montoya[32], J.R. Carter[30], J. Carvalho[127a,127c], D. Casadei[19], M.P. Casado[13,h], M. Casolino[13], D.W. Casper[163], E. Castaneda-Miranda[146a], R. Castelijn[108], A. Castelli[108], V. Castillo Gimenez[167], N.F. Castro[127a,i], A. Catinaccio[32], J.R. Catmore[120], A. Cattai[32], J. Caudron[85], V. Cavaliere[166], E. Cavallaro[13], D. Cavalli[93a], M. Cavalli-Sforza[13], V. Cavasinni[125a,125b], F. Ceradini[135a,135b], L. Cerda Alberich[167], B.C. Cerio[47], A.S. Cerqueira[26b], A. Cerri[150], L. Cerrito[78], F. Cerutti[16], M. Cerv[32], A. Cervelli[18], S.A. Cetin[20d], A. Chafaq[136a], D. Chakraborty[109], S.K. Chan[59], Y.L. Chan[62a], P. Chang[166], J.D. Chapman[30], D.G. Charlton[19], A. Chatterjee[51], C.C. Chau[159], C.A. Chavez Barajas[150], S. Che[112], S. Cheatham[74], A. Chegwidden[92], S. Chekanov[6], S.V. Chekulaev[160a], G.A. Chelkov[67,j], M.A. Chelstowska[91], C. Chen[66], H. Chen[27], K. Chen[149], S. Chen[35c], S. Chen[156], X. Chen[35f], Y. Chen[69], H.C. Cheng[91], H.J Cheng[35a], Y. Cheng[33], A. Cheplakov[67], E. Cheremushkina[131], R. Cherkaoui El Moursli[136e], V. Chernyatin[27,*], E. Cheu[7], L. Chevalier[137], V. Chiarella[49], G. Chiarelli[125a,125b], G. Chiodini[75a], A.S. Chisholm[19], A. Chitan[28b], M.V. Chizhov[67], K. Choi[63], A.R. Chomont[36], S. Chouridou[9], B.K.B. Chow[101], V. Christodoulou[80], D. Chromek-Burckhart[32], J. Chudoba[128], A.J. Chuinard[89], J.J. Chwastowski[41], L. Chytka[116], G. Ciapetti[133a,133b], A.K. Ciftci[4a], D. Cinca[55], V. Cindro[77], I.A. Cioara[23], A. Ciocio[16], F. Cirotto[105a,105b], Z.H. Citron[172], M. Citterio[93a], M. Ciubancan[28b], A. Clark[51], B.L. Clark[59], M.R. Clark[37], P.J. Clark[48], R.N. Clarke[16], C. Clement[147a,147b], Y. Coadou[87], M. Cobal[164a,164c], A. Coccaro[51], J. Cochran[66], L. Coffey[25], L. Colasurdo[107], B. Cole[37], A.P. Colijn[108], J. Collot[57], T. Colombo[32], G. Compostella[102], P. Conde Muiño[127a,127b], E. Coniavitis[50], S.H. Connell[146b], I.A. Connelly[79], V. Consorti[50], S. Constantinescu[28b], G. Conti[32], F. Conventi[105a,k], M. Cooke[16], B.D. Cooper[80], A.M. Cooper-Sarkar[121], K.J.R. Cormier[159], T. Cornelissen[175], M. Corradi[133a,133b], F. Corriveau[89,l], A. Corso-Radu[163], A. Cortes-Gonzalez[13], G. Cortiana[102], G. Costa[93a], M.J. Costa[167], D. Costanzo[140], G. Cottin[30], G. Cowan[79], B.E. Cox[86], K. Cranmer[111], S.J. Crawley[55], G. Cree[31], S. Crépé-Renaudin[57], F. Crescioli[82], W.A. Cribbs[147a,147b], M. Crispin Ortuzar[121], M. Cristinziani[23], V. Croft[107], G. Crosetti[39a,39b],

T. Cuhadar Donszelmann[140], J. Cummings[176], M. Curatolo[49], J. Cúth[85], C. Cuthbert[151], H. Czirr[142], P. Czodrowski[3], G. D'amen[22a,22b], S. D'Auria[55], M. D'Onofrio[76], M.J. Da Cunha Sargedas De Sousa[127a,127b], C. Da Via[86], W. Dabrowski[40a], T. Dado[145a], T. Dai[91], O. Dale[15], F. Dallaire[96], C. Dallapiccola[88], M. Dam[38], J.R. Dandoy[33], N.P. Dang[50], A.C. Daniells[19], N.S. Dann[86], M. Danninger[168], M. Dano Hoffmann[137], V. Dao[50], G. Darbo[52a], S. Darmora[8], J. Dassoulas[3], A. Dattagupta[63], W. Davey[23], C. David[169], T. Davidek[130], M. Davies[154], P. Davison[80], E. Dawe[90], I. Dawson[140], R.K. Daya-Ishmukhametova[88], K. De[8], R. de Asmundis[105a], A. De Benedetti[114], S. De Castro[22a,22b], S. De Cecco[82], N. De Groot[107], P. de Jong[108], H. De la Torre[84], F. De Lorenzi[66], A. De Maria[56], D. De Pedis[133a], A. De Salvo[133a], U. De Sanctis[150], A. De Santo[150], J.B. De Vivie De Regie[118], W.J. Dearnaley[74], R. Debbe[27], C. Debenedetti[138], D.V. Dedovich[67], N. Dehghanian[3], I. Deigaard[108], M. Del Gaudio[39a,39b], J. Del Peso[84], T. Del Prete[125a,125b], D. Delgove[118], F. Deliot[137], C.M. Delitzsch[51], M. Deliyergiyev[77], A. Dell'Acqua[32], L. Dell'Asta[24], M. Dell'Orso[125a,125b], M. Della Pietra[105a,k], D. della Volpe[51], M. Delmastro[5], P.A. Delsart[57], C. Deluca[108], D.A. DeMarco[159], S. Demers[176], M. Demichev[67], A. Demilly[82], S.P. Denisov[131], D. Denysiuk[137], D. Derendarz[41], J.E. Derkaoui[136d], F. Derue[82], P. Dervan[76], K. Desch[23], C. Deterre[44], K. Dette[45], P.O. Deviveiros[32], A. Dewhurst[132], S. Dhaliwal[25], A. Di Ciaccio[134a,134b], L. Di Ciaccio[5], W.K. Di Clemente[123], C. Di Donato[133a,133b], A. Di Girolamo[32], B. Di Girolamo[32], B. Di Micco[135a,135b], R. Di Nardo[32], A. Di Simone[50], R. Di Sipio[159], D. Di Valentino[31], C. Diaconu[87], M. Diamond[159], F.A. Dias[48], M.A. Diaz[34a], E.B. Diehl[91], J. Dietrich[17], S. Diglio[87], A. Dimitrievska[14], J. Dingfelder[23], P. Dita[28b], S. Dita[28b], F. Dittus[32], F. Djama[87], T. Djobava[53b], J.I. Djuvsland[60a], M.A.B. do Vale[26c], D. Dobos[32], M. Dobre[28b], C. Doglioni[83], T. Dohmae[156], J. Dolejsi[130], Z. Dolezal[130], B.A. Dolgoshein[99,*], M. Donadelli[26d], S. Donati[125a,125b], P. Dondero[122a,122b], J. Donini[36], J. Dopke[132], A. Doria[105a], M.T. Dova[73], A.T. Doyle[55], E. Drechsler[56], M. Dris[10], Y. Du[35d], J. Duarte-Campderros[154], E. Duchovni[172], G. Duckeck[101], O.A. Ducu[96,m], D. Duda[108], A. Dudarev[32], E.M. Duffield[16], L. Duflot[118], L. Duguid[79], M. Dührssen[32], M. Dumancic[172], M. Dunford[60a], H. Duran Yildiz[4a], M. Düren[54], A. Durglishvili[53b], D. Duschinger[46], B. Dutta[44], M. Dyndal[44], C. Eckardt[44], K.M. Ecker[102], R.C. Edgar[91], N.C. Edwards[48], T. Eifert[32], G. Eigen[15], K. Einsweiler[16], T. Ekelof[165], M. El Kacimi[136c], V. Ellajosyula[87], M. Ellert[165], S. Elles[5], F. Ellinghaus[175], A.A. Elliot[169], N. Ellis[32], J. Elmsheuser[27], M. Elsing[32], D. Emeliyanov[132], Y. Enari[156], O.C. Endner[85], M. Endo[119], J.S. Ennis[170], J. Erdmann[45], A. Ereditato[18], G. Ernis[175], J. Ernst[2], M. Ernst[27], S. Errede[166], E. Ertel[85], M. Escalier[118], H. Esch[45], C. Escobar[126], B. Esposito[49], A.I. Etienvre[137], E. Etzion[154], H. Evans[63], A. Ezhilov[124], F. Fabbri[22a,22b], L. Fabbri[22a,22b], G. Facini[33], R.M. Fakhrutdinov[131], S. Falciano[133a], R.J. Falla[80], J. Faltova[130], Y. Fang[35a], M. Fanti[93a,93b], A. Farbin[8], A. Farilla[135a], C. Farina[126], T. Farooque[13], S. Farrell[16], S.M. Farrington[170], P. Farthouat[32], F. Fassi[136e], P. Fassnacht[32], D. Fassouliotis[9], M. Faucci Giannelli[79], A. Favareto[52a,52b], W.J. Fawcett[121], L. Fayard[118], O.L. Fedin[124,n], W. Fedorko[168], S. Feigl[120], L. Feligioni[87], C. Feng[35d], E.J. Feng[32], H. Feng[91], A.B. Fenyuk[131], L. Feremenga[8], P. Fernandez Martinez[167], S. Fernandez Perez[13], J. Ferrando[55], A. Ferrari[165], P. Ferrari[108], R. Ferrari[122a], D.E. Ferreira de Lima[60b], A. Ferrer[167], D. Ferrere[51], C. Ferretti[91], A. Ferretto Parodi[52a,52b], F. Fiedler[85], A. Filipčič[77], M. Filipuzzi[44], F. Filthaut[107], M. Fincke-Keeler[169], K.D. Finelli[151], M.C.N. Fiolhais[127a,127c], L. Fiorini[167], A. Firan[42], A. Fischer[2], C. Fischer[13], J. Fischer[175], W.C. Fisher[92], N. Flaschel[44], I. Fleck[142], P. Fleischmann[91], G.T. Fletcher[140], R.R.M. Fletcher[123], T. Flick[175], A. Floderus[83], L.R. Flores Castillo[62a], M.J. Flowerdew[102], G.T. Forcolin[86], A. Formica[137], A. Forti[86], A.G. Foster[19], D. Fournier[118], H. Fox[74], S. Fracchia[13], P. Francavilla[82], M. Franchini[22a,22b], D. Francis[32], L. Franconi[120], M. Franklin[59], M. Frate[163], M. Fraternali[122a,122b], D. Freeborn[80], S.M. Fressard-Batraneanu[32], F. Friedrich[46], D. Froidevaux[32], J.A. Frost[121], C. Fukunaga[157], E. Fullana Torregrosa[85], T. Fusayasu[103], J. Fuster[167], C. Gabaldon[57], O. Gabizon[175], A. Gabrielli[22a,22b], A. Gabrielli[16], G.P. Gach[40a], S. Gadatsch[32], S. Gadomski[51], G. Gagliardi[52a,52b], L.G. Gagnon[96],

P. Gagnon[63], C. Galea[107], B. Galhardo[127a,127c], E.J. Gallas[121], B.J. Gallop[132], P. Gallus[129], G. Galster[38], K.K. Gan[112], J. Gao[35b,87], Y. Gao[48], Y.S. Gao[144,f], F.M. Garay Walls[48], C. García[167], J.E. García Navarro[167], M. Garcia-Sciveres[16], R.W. Gardner[33], N. Garelli[144], V. Garonne[120], A. Gascon Bravo[44], C. Gatti[49], A. Gaudiello[52a,52b], G. Gaudio[122a], B. Gaur[142], L. Gauthier[96], I.L. Gavrilenko[97], C. Gay[168], G. Gaycken[23], E.N. Gazis[10], Z. Gecse[168], C.N.P. Gee[132], Ch. Geich-Gimbel[23], M. Geisen[85], M.P. Geisler[60a], C. Gemme[52a], M.H. Genest[57], C. Geng[35b,o], S. Gentile[133a,133b], S. George[79], D. Gerbaudo[13], A. Gershon[154], S. Ghasemi[142], H. Ghazlane[136b], M. Ghneimat[23], B. Giacobbe[22a], S. Giagu[133a,133b], P. Giannetti[125a,125b], B. Gibbard[27], S.M. Gibson[79], M. Gignac[168], M. Gilchriese[16], T.P.S. Gillam[30], D. Gillberg[31], G. Gilles[175], D.M. Gingrich[3,d], N. Giokaris[9], M.P. Giordani[164a,164c], F.M. Giorgi[22a], F.M. Giorgi[17], P.F. Giraud[137], P. Giromini[59], D. Giugni[93a], F. Giuli[121], C. Giuliani[102], M. Giulini[60b], B.K. Gjelsten[120], S. Gkaitatzis[155], I. Gkialas[155], E.L. Gkougkousis[118], L.K. Gladilin[100], C. Glasman[84], J. Glatzer[32], P.C.F. Glaysher[48], A. Glazov[44], M. Goblirsch-Kolb[102], J. Godlewski[41], S. Goldfarb[91], T. Golling[51], D. Golubkov[131], A. Gomes[127a,127b,127d], R. Gonçalo[127a], J. Goncalves Pinto Firmino Da Costa[137], G. Gonella[50], L. Gonella[19], A. Gongadze[67], S. González de la Hoz[167], G. Gonzalez Parra[13], S. Gonzalez-Sevilla[51], L. Goossens[32], P.A. Gorbounov[98], H.A. Gordon[27], I. Gorelov[106], B. Gorini[32], E. Gorini[75a,75b], A. Gorišek[77], E. Gornicki[41], A.T. Goshaw[47], C. Gössling[45], M.I. Gostkin[67], C.R. Goudet[118], D. Goujdami[136c], A.G. Goussiou[139], N. Govender[146b,p], E. Gozani[153], L. Graber[56], I. Grabowska-Bold[40a], P.O.J. Gradin[57], P. Grafström[22a,22b], J. Gramling[51], E. Gramstad[120], S. Grancagnolo[17], V. Gratchev[124], P.M. Gravila[28e], H.M. Gray[32], E. Graziani[135a], Z.D. Greenwood[81,q], C. Grefe[23], K. Gregersen[80], I.M. Gregor[44], P. Grenier[144], K. Grevtsov[5], J. Griffiths[8], A.A. Grillo[138], K. Grimm[74], S. Grinstein[13,r], Ph. Gris[36], J.-F. Grivaz[118], S. Groh[85], J.P. Grohs[46], E. Gross[172], J. Grosse-Knetter[56], G.C. Grossi[81], Z.J. Grout[150], L. Guan[91], W. Guan[173], J. Guenther[129], F. Guescini[51], D. Guest[163], O. Gueta[154], E. Guido[52a,52b], T. Guillemin[5], S. Guindon[2], U. Gul[55], C. Gumpert[32], J. Guo[35e], Y. Guo[35b,o], S. Gupta[121], G. Gustavino[133a,133b], P. Gutierrez[114], N.G. Gutierrez Ortiz[80], C. Gutschow[46], C. Guyot[137], C. Gwenlan[121], C.B. Gwilliam[76], A. Haas[111], C. Haber[16], H.K. Hadavand[8], N. Haddad[136e], A. Hadef[87], P. Haefner[23], S. Hageböck[23], Z. Hajduk[41], H. Hakobyan[177,*], M. Haleem[44], J. Haley[115], G. Halladjian[92], G.D. Hallewell[87], K. Hamacher[175], P. Hamal[116], K. Hamano[169], A. Hamilton[146a], G.N. Hamity[140], P.G. Hamnett[44], L. Han[35b], K. Hanagaki[68,s], K. Hanawa[156], M. Hance[138], B. Haney[123], P. Hanke[60a], R. Hanna[137], J.B. Hansen[38], J.D. Hansen[38], M.C. Hansen[23], P.H. Hansen[38], K. Hara[161], A.S. Hard[173], T. Harenberg[175], F. Hariri[118], S. Harkusha[94], R.D. Harrington[48], P.F. Harrison[170], F. Hartjes[108], N.M. Hartmann[101], M. Hasegawa[69], Y. Hasegawa[141], A. Hasib[114], S. Hassani[137], S. Haug[18], R. Hauser[92], L. Hauswald[46], M. Havranek[128], C.M. Hawkes[19], R.J. Hawkings[32], D. Hayden[92], C.P. Hays[121], J.M. Hays[78], H.S. Hayward[76], S.J. Haywood[132], S.J. Head[19], T. Heck[85], V. Hedberg[83], L. Heelan[8], S. Heim[123], T. Heim[16], B. Heinemann[16], J.J. Heinrich[101], L. Heinrich[111], C. Heinz[54], J. Hejbal[128], L. Helary[24], S. Hellman[147a,147b], C. Helsens[32], J. Henderson[121], R.C.W. Henderson[74], Y. Heng[173], S. Henkelmann[168], A.M. Henriques Correia[32], S. Henrot-Versille[118], G.H. Herbert[17], Y. Hernández Jiménez[167], G. Herten[50], R. Hertenberger[101], L. Hervas[32], G.G. Hesketh[80], N.P. Hessey[108], J.W. Hetherly[42], R. Hickling[78], E. Higón-Rodriguez[167], E. Hill[169], J.C. Hill[30], K.H. Hiller[44], S.J. Hillier[19], I. Hinchliffe[16], E. Hines[123], R.R. Hinman[16], M. Hirose[158], D. Hirschbuehl[175], J. Hobbs[149], N. Hod[160a], M.C. Hodgkinson[140], P. Hodgson[140], A. Hoecker[32], M.R. Hoeferkamp[106], F. Hoenig[101], D. Hohn[23], T.R. Holmes[16], M. Homann[45], T.M. Hong[126], B.H. Hooberman[166], W.H. Hopkins[117], Y. Horii[104], A.J. Horton[143], J-Y. Hostachy[57], S. Hou[152], A. Hoummada[136a], J. Howarth[44], M. Hrabovsky[116], I. Hristova[17], J. Hrivnac[118], T. Hryn'ova[5], A. Hrynevich[95], C. Hsu[146c], P.J. Hsu[152,t], S.-C. Hsu[139], D. Hu[37], Q. Hu[35b], Y. Huang[44], Z. Hubacek[129], F. Hubaut[87], F. Huegging[23], T.B. Huffman[121], E.W. Hughes[37], G. Hughes[74], M. Huhtinen[32], T.A. Hülsing[85], P. Huo[149], N. Huseynov[67,b], J. Huston[92], J. Huth[59], G. Iacobucci[51],

G. Iakovidis[27], I. Ibragimov[142], L. Iconomidou-Fayard[118], E. Ideal[176], Z. Idrissi[136e], P. Iengo[32], O. Igonkina[108,u], T. Iizawa[171], Y. Ikegami[68], M. Ikeno[68], Y. Ilchenko[11,v], D. Iliadis[155], N. Ilic[144], T. Ince[102], G. Introzzi[122a,122b], P. Ioannou[9,*], M. Iodice[135a], K. Iordanidou[37], V. Ippolito[59], M. Ishino[70], M. Ishitsuka[158], R. Ishmukhametov[112], C. Issever[121], S. Istin[20a], F. Ito[161], J.M. Iturbe Ponce[86], R. Iuppa[134a,134b], W. Iwanski[41], H. Iwasaki[68], J.M. Izen[43], V. Izzo[105a], S. Jabbar[3], B. Jackson[123], M. Jackson[76], P. Jackson[1], V. Jain[2], K.B. Jakobi[85], K. Jakobs[50], S. Jakobsen[32], T. Jakoubek[128], D.O. Jamin[115], D.K. Jana[81], E. Jansen[80], R. Jansky[64], J. Janssen[23], M. Janus[56], G. Jarlskog[83], N. Javadov[67,b], T. Javůrek[50], F. Jeanneau[137], L. Jeanty[16], J. Jejelava[53a,w], G.-Y. Jeng[151], D. Jennens[90], P. Jenni[50,x], J. Jentzsch[45], C. Jeske[170], S. Jézéquel[5], H. Ji[173], J. Jia[149], H. Jiang[66], Y. Jiang[35b], S. Jiggins[80], J. Jimenez Pena[167], S. Jin[35a], A. Jinaru[28b], O. Jinnouchi[158], P. Johansson[140], K.A. Johns[7], W.J. Johnson[139], K. Jon-And[147a,147b], G. Jones[170], R.W.L. Jones[74], S. Jones[7], T.J. Jones[76], J. Jongmanns[60a], P.M. Jorge[127a,127b], J. Jovicevic[160a], X. Ju[173], A. Juste Rozas[13,r], M.K. Köhler[172], A. Kaczmarska[41], M. Kado[118], H. Kagan[112], M. Kagan[144], S.J. Kahn[87], E. Kajomovitz[47], C.W. Kalderon[121], A. Kaluza[85], S. Kama[42], A. Kamenshchikov[131], N. Kanaya[156], S. Kaneti[30], L. Kanjir[77], V.A. Kantserov[99], J. Kanzaki[68], B. Kaplan[111], L.S. Kaplan[173], A. Kapliy[33], D. Kar[146c], K. Karakostas[10], A. Karamaoun[3], N. Karastathis[10], M.J. Kareem[56], E. Karentzos[10], M. Karnevskiy[85], S.N. Karpov[67], Z.M. Karpova[67], K. Karthik[111], V. Kartvelishvili[74], A.N. Karyukhin[131], K. Kasahara[161], L. Kashif[173], R.D. Kass[112], A. Kastanas[15], Y. Kataoka[156], C. Kato[156], A. Katre[51], J. Katzy[44], K. Kawagoe[72], T. Kawamoto[156], G. Kawamura[56], S. Kazama[156], V.F. Kazanin[110,c], R. Keeler[169], R. Kehoe[42], J.S. Keller[44], J.J. Kempster[79], K Kentaro[104], H. Keoshkerian[159], O. Kepka[128], B.P. Kerševan[77], S. Kersten[175], R.A. Keyes[89], F. Khalil-zada[12], A. Khanov[115], A.G. Kharlamov[110,c], T.J. Khoo[51], V. Khovanskiy[98], E. Khramov[67], J. Khubua[53b,y], S. Kido[69], H.Y. Kim[8], S.H. Kim[161], Y.K. Kim[33], N. Kimura[155], O.M. Kind[17], B.T. King[76], M. King[167], S.B. King[168], J. Kirk[132], A.E. Kiryunin[102], T. Kishimoto[69], D. Kisielewska[40a], F. Kiss[50], K. Kiuchi[161], O. Kivernyk[137], E. Kladiva[145b], M.H. Klein[37], M. Klein[76], U. Klein[76], K. Kleinknecht[85], P. Klimek[147a,147b], A. Klimentov[27], R. Klingenberg[45], J.A. Klinger[140], T. Klioutchnikova[32], E.-E. Kluge[60a], P. Kluit[108], S. Kluth[102], J. Knapik[41], E. Kneringer[64], E.B.F.G. Knoops[87], A. Knue[55], A. Kobayashi[156], D. Kobayashi[158], T. Kobayashi[156], M. Kobel[46], M. Kocian[144], P. Kodys[130], T. Koffas[31], E. Koffeman[108], T. Koi[144], H. Kolanoski[17], M. Kolb[60b], I. Koletsou[5], A.A. Komar[97,*], Y. Komori[156], T. Kondo[68], N. Kondrashova[44], K. Köneke[50], A.C. König[107], T. Kono[68,z], R. Konoplich[111,aa], N. Konstantinidis[80], R. Kopeliansky[63], S. Koperny[40a], L. Köpke[85], A.K. Kopp[50], K. Korcyl[41], K. Kordas[155], A. Korn[80], A.A. Korol[110,c], I. Korolkov[13], E.V. Korolkova[140], O. Kortner[102], S. Kortner[102], T. Kosek[130], V.V. Kostyukhin[23], A. Kotwal[47], A. Kourkoumeli-Charalampidi[155], C. Kourkoumelis[9], V. Kouskoura[27], A.B. Kowalewska[41], R. Kowalewski[169], T.Z. Kowalski[40a], C. Kozakai[156], W. Kozanecki[137], A.S. Kozhin[131], V.A. Kramarenko[100], G. Kramberger[77], D. Krasnopevtsev[99], M.W. Krasny[82], A. Krasznahorkay[32], J.K. Kraus[23], A. Kravchenko[27], M. Kretz[60c], J. Kretzschmar[76], K. Kreutzfeldt[54], P. Krieger[159], K. Krizka[33], K. Kroeninger[45], H. Kroha[102], J. Kroll[123], J. Kroseberg[23], J. Krstic[14], U. Kruchonak[67], H. Krüger[23], N. Krumnack[66], A. Kruse[173], M.C. Kruse[47], M. Kruskal[24], T. Kubota[90], H. Kucuk[80], S. Kuday[4b], J.T. Kuechler[175], S. Kuehn[50], A. Kugel[60c], F. Kuger[174], A. Kuhl[138], T. Kuhl[44], V. Kukhtin[67], R. Kukla[137], Y. Kulchitsky[94], S. Kuleshov[34b], M. Kuna[133a,133b], T. Kunigo[70], A. Kupco[128], H. Kurashige[69], Y.A. Kurochkin[94], V. Kus[128], E.S. Kuwertz[169], M. Kuze[158], J. Kvita[116], T. Kwan[169], D. Kyriazopoulos[140], A. La Rosa[102], J.L. La Rosa Navarro[26d], L. La Rotonda[39a,39b], C. Lacasta[167], F. Lacava[133a,133b], J. Lacey[31], H. Lacker[17], D. Lacour[82], V.R. Lacuesta[167], E. Ladygin[67], R. Lafaye[5], B. Laforge[82], T. Lagouri[176], S. Lai[56], S. Lammers[63], W. Lampl[7], E. Lançon[137], U. Landgraf[50], M.P.J. Landon[78], V.S. Lang[60a], J.C. Lange[13], A.J. Lankford[163], F. Lanni[27], K. Lantzsch[23], A. Lanza[122a], S. Laplace[82], C. Lapoire[32], J.F. Laporte[137], T. Lari[93a], F. Lasagni Manghi[22a,22b], M. Lassnig[32], P. Laurelli[49], W. Lavrijsen[16], A.T. Law[138], P. Laycock[76], T. Lazovich[59], M. Lazzaroni[93a,93b], B. Le[90],

O. Le Dortz[82], E. Le Guirriec[87], E.P. Le Quilleuc[137], M. LeBlanc[169], T. LeCompte[6], F. Ledroit-Guillon[57], C.A. Lee[27], S.C. Lee[152], L. Lee[1], G. Lefebvre[82], M. Lefebvre[169], F. Legger[101], C. Leggett[16], A. Lehan[76], G. Lehmann Miotto[32], X. Lei[7], W.A. Leight[31], A. Leisos[155,ab], A.G. Leister[176], M.A.L. Leite[26d], R. Leitner[130], D. Lellouch[172], B. Lemmer[56], K.J.C. Leney[80], T. Lenz[23], B. Lenzi[32], R. Leone[7], S. Leone[125a,125b], C. Leonidopoulos[48], S. Leontsinis[10], G. Lerner[150], C. Leroy[96], A.A.J. Lesage[137], C.G. Lester[30], M. Levchenko[124], J. Levêque[5], D. Levin[91], L.J. Levinson[172], M. Levy[19], D. Lewis[78], A.M. Leyko[23], M. Leyton[43], B. Li[35b,o], H. Li[149], H.L. Li[33], L. Li[47], L. Li[35e], Q. Li[35a], S. Li[47], X. Li[86], Y. Li[142], Z. Liang[35a], B. Liberti[134a], A. Liblong[159], P. Lichard[32], K. Lie[166], J. Liebal[23], W. Liebig[15], A. Limosani[151], S.C. Lin[152,ac], T.H. Lin[85], B.E. Lindquist[149], A.E. Lionti[51], E. Lipeles[123], A. Lipniacka[15], M. Lisovyi[60b], T.M. Liss[166], A. Lister[168], A.M. Litke[138], B. Liu[152,ad], D. Liu[152], H. Liu[91], H. Liu[27], J. Liu[87], J.B. Liu[35b], K. Liu[87], L. Liu[166], M. Liu[47], M. Liu[35b], Y.L. Liu[35b], Y. Liu[35b], M. Livan[122a,122b], A. Lleres[57], J. Llorente Merino[35a], S.L. Lloyd[78], F. Lo Sterzo[152], E. Lobodzinska[44], P. Loch[7], W.S. Lockman[138], F.K. Loebinger[86], A.E. Loevschall-Jensen[38], K.M. Loew[25], A. Loginov[176], T. Lohse[17], K. Lohwasser[44], M. Lokajicek[128], B.A. Long[24], J.D. Long[166], R.E. Long[74], L. Longo[75a,75b], K.A. Looper[112], L. Lopes[127a], D. Lopez Mateos[59], B. Lopez Paredes[140], I. Lopez Paz[13], A. Lopez Solis[82], J. Lorenz[101], N. Lorenzo Martinez[63], M. Losada[21], P.J. Lösel[101], X. Lou[35a], A. Lounis[118], J. Love[6], P.A. Love[74], H. Lu[62a], N. Lu[91], H.J. Lubatti[139], C. Luci[133a,133b], A. Lucotte[57], C. Luedtke[50], F. Luehring[63], W. Lukas[64], L. Luminari[133a], O. Lundberg[147a,147b], B. Lund-Jensen[148], P.M. Luzi[82], D. Lynn[27], R. Lysak[128], E. Lytken[83], V. Lyubushkin[67], H. Ma[27], L.L. Ma[35d], Y. Ma[35d], G. Maccarrone[49], A. Macchiolo[102], C.M. Macdonald[140], B. Maček[77], J. Machado Miguens[123,127b], D. Madaffari[87], R. Madar[36], H.J. Maddocks[165], W.F. Mader[46], A. Madsen[44], J. Maeda[69], S. Maeland[15], T. Maeno[27], A. Maevskiy[100], E. Magradze[56], J. Mahlstedt[108], C. Maiani[118], C. Maidantchik[26a], A.A. Maier[102], T. Maier[101], A. Maio[127a,127b,127d], S. Majewski[117], Y. Makida[68], N. Makovec[118], B. Malaescu[82], Pa. Malecki[41], V.P. Maleev[124], F. Malek[57], U. Mallik[65], D. Malon[6], C. Malone[144], S. Maltezos[10], S. Malyukov[32], J. Mamuzic[167], G. Mancini[49], B. Mandelli[32], L. Mandelli[93a], I. Mandić[77], J. Maneira[127a,127b], L. Manhaes de Andrade Filho[26b], J. Manjarres Ramos[160b], A. Mann[101], A. Manousos[32], B. Mansoulie[137], J.D. Mansour[35a], R. Mantifel[89], M. Mantoani[56], S. Manzoni[93a,93b], L. Mapelli[32], G. Marceca[29], L. March[51], G. Marchiori[82], M. Marcisovsky[128], M. Marjanovic[14], D.E. Marley[91], F. Marroquim[26a], S.P. Marsden[86], Z. Marshall[16], S. Marti-Garcia[167], B. Martin[92], T.A. Martin[170], V.J. Martin[48], B. Martin dit Latour[15], M. Martinez[13,r], S. Martin-Haugh[132], V.S. Martoiu[28b], A.C. Martyniuk[80], M. Marx[139], A. Marzin[32], L. Masetti[85], T. Mashimo[156], R. Mashinistov[97], J. Masik[86], A.L. Maslennikov[110,c], I. Massa[22a,22b], L. Massa[22a,22b], P. Mastrandrea[5], A. Mastroberardino[39a,39b], T. Masubuchi[156], P. Mättig[175], J. Mattmann[85], J. Maurer[28b], S.J. Maxfield[76], D.A. Maximov[110,c], R. Mazini[152], S.M. Mazza[93a,93b], N.C. Mc Fadden[106], G. Mc Goldrick[159], S.P. Mc Kee[91], A. McCarn[91], R.L. McCarthy[149], T.G. McCarthy[102], L.I. McClymont[80], E.F. McDonald[90], K.W. McFarlane[58,*], J.A. Mcfayden[80], G. Mchedlidze[56], S.J. McMahon[132], R.A. McPherson[169,l], M. Medinnis[44], S. Meehan[139], S. Mehlhase[101], A. Mehta[76], K. Meier[60a], C. Meineck[101], B. Meirose[43], D. Melini[167], B.R. Mellado Garcia[146c], M. Melo[145a], F. Meloni[18], A. Mengarelli[22a,22b], S. Menke[102], E. Meoni[162], S. Mergelmeyer[17], P. Mermod[51], L. Merola[105a,105b], C. Meroni[93a], F.S. Merritt[33], A. Messina[133a,133b], J. Metcalfe[6], A.S. Mete[163], C. Meyer[85], C. Meyer[123], J-P. Meyer[137], J. Meyer[108], H. Meyer Zu Theenhausen[60a], F. Miano[150], R.P. Middleton[132], S. Miglioranzi[52a,52b], L. Mijović[23], G. Mikenberg[172], M. Mikestikova[128], M. Mikuž[77], M. Milesi[90], A. Milic[64], D.W. Miller[33], C. Mills[48], A. Milov[172], D.A. Milstead[147a,147b], A.A. Minaenko[131], Y. Minami[156], I.A. Minashvili[67], A.I. Mincer[111], B. Mindur[40a], M. Mineev[67], Y. Ming[173], L.M. Mir[13], K.P. Mistry[123], T. Mitani[171], J. Mitrevski[101], V.A. Mitsou[167], A. Miucci[51], P.S. Miyagawa[140], J.U. Mjörnmark[83], T. Moa[147a,147b], K. Mochizuki[96], S. Mohapatra[37], S. Molander[147a,147b], R. Moles-Valls[23], R. Monden[70], M.C. Mondragon[92], K. Mönig[44], J. Monk[38],

E. Monnier[87], A. Montalbano[149], J. Montejo Berlingen[32], F. Monticelli[73], S. Monzani[93a,93b], R.W. Moore[3], N. Morange[118], D. Moreno[21], M. Moreno Llácer[56], P. Morettini[52a], D. Mori[143], T. Mori[156], M. Morii[59], M. Morinaga[156], V. Morisbak[120], S. Moritz[85], A.K. Morley[151], G. Mornacchi[32], J.D. Morris[78], S.S. Mortensen[38], L. Morvaj[149], M. Mosidze[53b], J. Moss[144], K. Motohashi[158], R. Mount[144], E. Mountricha[27], S.V. Mouraviev[97,*], E.J.W. Moyse[88], S. Muanza[87], R.D. Mudd[19], F. Mueller[102], J. Mueller[126], R.S.P. Mueller[101], T. Mueller[30], D. Muenstermann[74], P. Mullen[55], G.A. Mullier[18], F.J. Munoz Sanchez[86], J.A. Murillo Quijada[19], W.J. Murray[170,132], H. Musheghyan[56], M. Muškinja[77], A.G. Myagkov[131,*ae*], M. Myska[129], B.P. Nachman[144], O. Nackenhorst[51], K. Nagai[121], R. Nagai[68,*z*], K. Nagano[68], Y. Nagasaka[61], K. Nagata[161], M. Nagel[50], E. Nagy[87], A.M. Nairz[32], Y. Nakahama[32], K. Nakamura[68], T. Nakamura[156], I. Nakano[113], H. Namasivayam[43], R.F. Naranjo Garcia[44], R. Narayan[11], D.I. Narrias Villar[60a], I. Naryshkin[124], T. Naumann[44], G. Navarro[21], R. Nayyar[7], H.A. Neal[91], P.Yu. Nechaeva[97], T.J. Neep[86], P.D. Nef[144], A. Negri[122a,122b], M. Negrini[22a], S. Nektarijevic[107], C. Nellist[118], A. Nelson[163], S. Nemecek[128], P. Nemethy[111], A.A. Nepomuceno[26a], M. Nessi[32,*af*], M.S. Neubauer[166], M. Neumann[175], R.M. Neves[111], P. Nevski[27], P.R. Newman[19], D.H. Nguyen[6], T. Nguyen Manh[96], R.B. Nickerson[121], R. Nicolaidou[137], J. Nielsen[138], A. Nikiforov[17], V. Nikolaenko[131,*ae*], I. Nikolic-Audit[82], K. Nikolopoulos[19], J.K. Nilsen[120], P. Nilsson[27], Y. Ninomiya[156], A. Nisati[133a], R. Nisius[102], T. Nobe[156], L. Nodulman[6], M. Nomachi[119], I. Nomidis[31], T. Nooney[78], S. Norberg[114], M. Nordberg[32], N. Norjoharuddeen[121], O. Novgorodova[46], S. Nowak[102], M. Nozaki[68], L. Nozka[116], K. Ntekas[10], E. Nurse[80], F. Nuti[90], F. O'grady[7], D.C. O'Neil[143], A.A. O'Rourke[44], V. O'Shea[55], F.G. Oakham[31,*d*], H. Oberlack[102], T. Obermann[23], J. Ocariz[82], A. Ochi[69], I. Ochoa[37], J.P. Ochoa-Ricoux[34a], S. Oda[72], S. Odaka[68], H. Ogren[63], A. Oh[86], S.H. Oh[47], C.C. Ohm[16], H. Ohman[165], H. Oide[32], H. Okawa[161], Y. Okumura[33], T. Okuyama[68], A. Olariu[28b], L.F. Oleiro Seabra[127a], S.A. Olivares Pino[48], D. Oliveira Damazio[27], A. Olszewski[41], J. Olszowska[41], A. Onofre[127a,127e], K. Onogi[104], P.U.E. Onyisi[11,*v*], M.J. Oreglia[33], Y. Oren[154], D. Orestano[135a,135b], N. Orlando[62b], R.S. Orr[159], B. Osculati[52a,52b], R. Ospanov[86], G. Otero y Garzon[29], H. Otono[72], M. Ouchrif[136d], F. Ould-Saada[120], A. Ouraou[137], K.P. Oussoren[108], Q. Ouyang[35a], M. Owen[55], R.E. Owen[19], V.E. Ozcan[20a], N. Ozturk[8], K. Pachal[143], A. Pacheco Pages[13], C. Padilla Aranda[13], M. Pagáčová[50], S. Pagan Griso[16], F. Paige[27], P. Pais[88], K. Pajchel[120], G. Palacino[160b], S. Palestini[32], M. Palka[40b], D. Pallin[36], A. Palma[127a,127b], E.St. Panagiotopoulou[10], C.E. Pandini[82], J.G. Panduro Vazquez[79], P. Pani[147a,147b], S. Panitkin[27], D. Pantea[28b], L. Paolozzi[51], Th.D. Papadopoulou[10], K. Papageorgiou[155], A. Paramonov[6], D. Paredes Hernandez[176], A.J. Parker[74], M.A. Parker[30], K.A. Parker[140], F. Parodi[52a,52b], J.A. Parsons[37], U. Parzefall[50], V.R. Pascuzzi[159], E. Pasqualucci[133a], S. Passaggio[52a], Fr. Pastore[79], G. Pásztor[31,*ag*], S. Pataraia[175], J.R. Pater[86], T. Pauly[32], J. Pearce[169], B. Pearson[114], L.E. Pedersen[38], M. Pedersen[120], S. Pedraza Lopez[167], R. Pedro[127a,127b], S.V. Peleganchuk[110,*c*], D. Pelikan[165], O. Penc[128], C. Peng[35a], H. Peng[35b], J. Penwell[63], B.S. Peralva[26b], M.M. Perego[137], D.V. Perepelitsa[27], E. Perez Codina[160a], L. Perini[93a,93b], H. Pernegger[32], S. Perrella[105a,105b], R. Peschke[44], V.D. Peshekhonov[67], K. Peters[44], R.F.Y. Peters[86], B.A. Petersen[32], T.C. Petersen[38], E. Petit[57], A. Petridis[1], C. Petridou[155], P. Petroff[118], E. Petrolo[133a], M. Petrov[121], F. Petrucci[135a,135b], N.E. Pettersson[88], A. Peyaud[137], R. Pezoa[34b], P.W. Phillips[132], G. Piacquadio[144], E. Pianori[170], A. Picazio[88], E. Piccaro[78], M. Piccinini[22a,22b], M.A. Pickering[121], R. Piegaia[29], J.E. Pilcher[33], A.D. Pilkington[86], A.W.J. Pin[86], M. Pinamonti[164a,164c,*ah*], J.L. Pinfold[3], A. Pingel[38], S. Pires[82], H. Pirumov[44], M. Pitt[172], L. Plazak[145a], M.-A. Pleier[27], V. Pleskot[85], E. Plotnikova[67], P. Plucinski[92], D. Pluth[66], R. Poettgen[147a,147b], L. Poggioli[118], D. Pohl[23], G. Polesello[122a], A. Poley[44], A. Policicchio[39a,39b], R. Polifka[159], A. Polini[22a], C.S. Pollard[55], V. Polychronakos[27], K. Pommès[32], L. Pontecorvo[133a], B.G. Pope[92], G.A. Popeneciu[28c], D.S. Popovic[14], A. Poppleton[32], S. Pospisil[129], K. Potamianos[16], I.N. Potrap[67], C.J. Potter[30], C.T. Potter[117], G. Poulard[32], J. Poveda[32], V. Pozdnyakov[67], M.E. Pozo Astigarraga[32], P. Pralavorio[87], A. Pranko[16], S. Prell[66], D. Price[86],

L.E. Price[6], M. Primavera[75a], S. Prince[89], M. Proissl[48], K. Prokofiev[62c], F. Prokoshin[34b], S. Protopopescu[27], J. Proudfoot[6], M. Przybycien[40a], D. Puddu[135a,135b], M. Purohit[27,ai], P. Puzo[118], J. Qian[91], G. Qin[55], Y. Qin[86], A. Quadt[56], W.B. Quayle[164a,164b], M. Queitsch-Maitland[86], D. Quilty[55], S. Raddum[120], V. Radeka[27], V. Radescu[60b], S.K. Radhakrishnan[149], P. Radloff[117], P. Rados[90], F. Ragusa[93a,93b], G. Rahal[178], J.A. Raine[86], S. Rajagopalan[27], M. Rammensee[32], C. Rangel-Smith[165], M.G. Ratti[93a,93b], F. Rauscher[101], S. Rave[85], T. Ravenscroft[55], I. Ravinovich[172], M. Raymond[32], A.L. Read[120], N.P. Readioff[76], M. Reale[75a,75b], D.M. Rebuzzi[122a,122b], A. Redelbach[174], G. Redlinger[27], R. Reece[138], K. Reeves[43], L. Rehnisch[17], J. Reichert[123], H. Reisin[29], C. Rembser[32], H. Ren[35a], M. Rescigno[133a], S. Resconi[93a], O.L. Rezanova[110,c], P. Reznicek[130], R. Rezvani[96], R. Richter[102], S. Richter[80], E. Richter-Was[40b], O. Ricken[23], M. Ridel[82], P. Rieck[17], C.J. Riegel[175], J. Rieger[56], O. Rifki[114], M. Rijssenbeek[149], A. Rimoldi[122a,122b], M. Rimoldi[18], L. Rinaldi[22a], B. Ristić[51], E. Ritsch[32], I. Riu[13], F. Rizatdinova[115], E. Rizvi[78], C. Rizzi[13], S.H. Robertson[89,l], A. Robichaud-Veronneau[89], D. Robinson[30], J.E.M. Robinson[44], A. Robson[55], C. Roda[125a,125b], Y. Rodina[87], A. Rodriguez Perez[13], D. Rodriguez Rodriguez[167], S. Roe[32], C.S. Rogan[59], O. Røhne[120], A. Romaniouk[99], M. Romano[22a,22b], S.M. Romano Saez[36], E. Romero Adam[167], N. Rompotis[139], M. Ronzani[50], L. Roos[82], E. Ros[167], S. Rosati[133a], K. Rosbach[50], P. Rose[138], O. Rosenthal[142], N.-A. Rosien[56], V. Rossetti[147a,147b], E. Rossi[105a,105b], L.P. Rossi[52a], J.H.N. Rosten[30], R. Rosten[139], M. Rotaru[28b], I. Roth[172], J. Rothberg[139], D. Rousseau[118], C.R. Royon[137], A. Rozanov[87], Y. Rozen[153], X. Ruan[146c], F. Rubbo[144], M.S. Rudolph[159], F. Rühr[50], A. Ruiz-Martinez[31], Z. Rurikova[50], N.A. Rusakovich[67], A. Ruschke[101], H.L. Russell[139], J.P. Rutherfoord[7], N. Ruthmann[32], Y.F. Ryabov[124], M. Rybar[166], G. Rybkin[118], S. Ryu[6], A. Ryzhov[131], G.F. Rzehorz[56], A.F. Saavedra[151], G. Sabato[108], S. Sacerdoti[29], H.F-W. Sadrozinski[138], R. Sadykov[67], F. Safai Tehrani[133a], P. Saha[109], M. Sahinsoy[60a], M. Saimpert[137], T. Saito[156], H. Sakamoto[156], Y. Sakurai[171], G. Salamanna[135a,135b], A. Salamon[134a,134b], J.E. Salazar Loyola[34b], D. Salek[108], P.H. Sales De Bruin[139], D. Salihagic[102], A. Salnikov[144], J. Salt[167], D. Salvatore[39a,39b], F. Salvatore[150], A. Salvucci[62a], A. Salzburger[32], D. Sammel[50], D. Sampsonidis[155], A. Sanchez[105a,105b], J. Sánchez[167], V. Sanchez Martinez[167], H. Sandaker[120], R.L. Sandbach[78], H.G. Sander[85], M. Sandhoff[175], C. Sandoval[21], R. Sandstroem[102], D.P.C. Sankey[132], M. Sannino[52a,52b], A. Sansoni[49], C. Santoni[36], R. Santonico[134a,134b], H. Santos[127a], I. Santoyo Castillo[150], K. Sapp[126], A. Sapronov[67], J.G. Saraiva[127a,127d], B. Sarrazin[23], O. Sasaki[68], Y. Sasaki[156], K. Sato[161], G. Sauvage[5,*], E. Sauvan[5], G. Savage[79], P. Savard[159,d], C. Sawyer[132], L. Sawyer[81,q], J. Saxon[33], C. Sbarra[22a], A. Sbrizzi[22a,22b], T. Scanlon[80], D.A. Scannicchio[163], M. Scarcella[151], V. Scarfone[39a,39b], J. Schaarschmidt[172], P. Schacht[102], B.M. Schachtner[101], D. Schaefer[32], R. Schaefer[44], J. Schaeffer[85], S. Schaepe[23], S. Schaetzel[60b], U. Schäfer[85], A.C. Schaffer[118], D. Schaile[101], R.D. Schamberger[149], V. Scharf[60a], V.A. Schegelsky[124], D. Scheirich[130], M. Schernau[163], C. Schiavi[52a,52b], S. Schier[138], C. Schillo[50], M. Schioppa[39a,39b], S. Schlenker[32], K.R. Schmidt-Sommerfeld[102], K. Schmieden[32], C. Schmitt[85], S. Schmitt[44], S. Schmitz[85], B. Schneider[160a], U. Schnoor[50], L. Schoeffel[137], A. Schoening[60b], B.D. Schoenrock[92], E. Schopf[23], M. Schott[85], J. Schovancova[8], S. Schramm[51], M. Schreyer[174], N. Schuh[85], M.J. Schultens[23], H.-C. Schultz-Coulon[60a], H. Schulz[17], M. Schumacher[50], B.A. Schumm[138], Ph. Schune[137], A. Schwartzman[144], T.A. Schwarz[91], Ph. Schwegler[102], H. Schweiger[86], Ph. Schwemling[137], R. Schwienhorst[92], J. Schwindling[137], T. Schwindt[23], G. Sciolla[25], F. Scuri[125a,125b], F. Scutti[90], J. Searcy[91], P. Seema[23], S.C. Seidel[106], A. Seiden[138], F. Seifert[129], J.M. Seixas[26a], G. Sekhniaidze[105a], K. Sekhon[91], S.J. Sekula[42], D.M. Seliverstov[124,*], N. Semprini-Cesari[22a,22b], C. Serfon[120], L. Serin[118], L. Serkin[164a,164b], M. Sessa[135a,135b], R. Seuster[169], H. Severini[114], T. Sfiligoj[77], F. Sforza[32], A. Sfyrla[51], E. Shabalina[56], N.W. Shaikh[147a,147b], L.Y. Shan[35a], R. Shang[166], J.T. Shank[24], M. Shapiro[16], P.B. Shatalov[98], K. Shaw[164a,164b], S.M. Shaw[86], A. Shcherbakova[147a,147b], C.Y. Shehu[150], P. Sherwood[80], L. Shi[152,aj], S. Shimizu[69], C.O. Shimmin[163], M. Shimojima[103], M. Shiyakova[67,ak], A. Shmeleva[97], D. Shoaleh Saadi[96], M.J. Shochet[33],

S. Shojaii[93a,93b], S. Shrestha[112], E. Shulga[99], M.A. Shupe[7], P. Sicho[128], A.M. Sickles[166], P.E. Sidebo[148], O. Sidiropoulou[174], D. Sidorov[115], A. Sidoti[22a,22b], F. Siegert[46], Dj. Sijacki[14], J. Silva[127a,127d], S.B. Silverstein[147a], V. Simak[129], O. Simard[5], Lj. Simic[14], S. Simion[118], E. Simioni[85], B. Simmons[80], D. Simon[36], M. Simon[85], P. Sinervo[159], N.B. Sinev[117], M. Sioli[22a,22b], G. Siragusa[174], S.Yu. Sivoklokov[100], J. Sjölin[147a,147b], T.B. Sjursen[15], M.B. Skinner[74], H.P. Skottowe[59], P. Skubic[114], M. Slater[19], T. Slavicek[129], M. Slawinska[108], K. Sliwa[162], R. Slovak[130], V. Smakhtin[172], B.H. Smart[5], L. Smestad[15], J. Smiesko[145a], S.Yu. Smirnov[99], Y. Smirnov[99], L.N. Smirnova[100,*al*], O. Smirnova[83], M.N.K. Smith[37], R.W. Smith[37], M. Smizanska[74], K. Smolek[129], A.A. Snesarev[97], S. Snyder[27], R. Sobie[169,*l*], F. Socher[46], A. Soffer[154], D.A. Soh[152], G. Sokhrannyi[77], C.A. Solans Sanchez[32], M. Solar[129], E.Yu. Soldatov[99], U. Soldevila[167], A.A. Solodkov[131], A. Soloshenko[67], O.V. Solovyanov[131], V. Solovyev[124], P. Sommer[50], H. Son[162], H.Y. Song[35b,*am*], A. Sood[16], A. Sopczak[129], V. Sopko[129], V. Sorin[13], D. Sosa[60b], C.L. Sotiropoulou[125a,125b], R. Soualah[164a,164c], A.M. Soukharev[110,*c*], D. South[44], B.C. Sowden[79], S. Spagnolo[75a,75b], M. Spalla[125a,125b], M. Spangenberg[170], F. Spanò[79], D. Sperlich[17], F. Spettel[102], R. Spighi[22a], G. Spigo[32], L.A. Spiller[90], M. Spousta[130], R.D. St. Denis[55,*], A. Stabile[93a], R. Stamen[60a], S. Stamm[17], E. Stanecka[41], R.W. Stanek[6], C. Stanescu[135a], M. Stanescu-Bellu[44], M.M. Stanitzki[44], S. Stapnes[120], E.A. Starchenko[131], G.H. Stark[33], J. Stark[57], P. Staroba[128], P. Starovoitov[60a], S. Stärz[32], R. Staszewski[41], P. Steinberg[27], B. Stelzer[143], H.J. Stelzer[32], O. Stelzer-Chilton[160a], H. Stenzel[54], G.A. Stewart[55], J.A. Stillings[23], M.C. Stockton[89], M. Stoebe[89], G. Stoicea[28b], P. Stolte[56], S. Stonjek[102], A.R. Stradling[8], A. Straessner[46], M.E. Stramaglia[18], J. Strandberg[148], S. Strandberg[147a,147b], A. Strandlie[120], M. Strauss[114], P. Strizenec[145b], R. Ströhmer[174], D.M. Strom[117], R. Stroynowski[42], A. Strubig[107], S.A. Stucci[18], B. Stugu[15], N.A. Styles[44], D. Su[144], J. Su[126], R. Subramaniam[81], S. Suchek[60a], Y. Sugaya[119], M. Suk[129], V.V. Sulin[97], S. Sultansoy[4c], T. Sumida[70], S. Sun[59], X. Sun[35a], J.E. Sundermann[50], K. Suruliz[150], G. Susinno[39a,39b], M.R. Sutton[150], S. Suzuki[68], M. Svatos[128], M. Swiatlowski[33], I. Sykora[145a], T. Sykora[130], D. Ta[50], C. Taccini[135a,135b], K. Tackmann[44], J. Taenzer[159], A. Taffard[163], R. Tafirout[160a], N. Taiblum[154], H. Takai[27], R. Takashima[71], T. Takeshita[141], Y. Takubo[68], M. Talby[87], A.A. Talyshev[110,*c*], K.G. Tan[90], J. Tanaka[156], R. Tanaka[118], S. Tanaka[68], B.B. Tannenwald[112], S. Tapia Araya[34b], S. Tapprogge[85], S. Tarem[153], G.F. Tartarelli[93a], P. Tas[130], M. Tasevsky[128], T. Tashiro[70], E. Tassi[39a,39b], A. Tavares Delgado[127a,127b], Y. Tayalati[136d], A.C. Taylor[106], G.N. Taylor[90], P.T.E. Taylor[90], W. Taylor[160b], F.A. Teischinger[32], P. Teixeira-Dias[79], K.K. Temming[50], D. Temple[143], H. Ten Kate[32], P.K. Teng[152], J.J. Teoh[119], F. Tepel[175], S. Terada[68], K. Terashi[156], J. Terron[84], S. Terzo[102], M. Testa[49], R.J. Teuscher[159,*l*], T. Theveneaux-Pelzer[87], J.P. Thomas[19], J. Thomas-Wilsker[79], E.N. Thompson[37], P.D. Thompson[19], A.S. Thompson[55], L.A. Thomsen[176], E. Thomson[123], M. Thomson[30], M.J. Tibbetts[16], R.E. Ticse Torres[87], V.O. Tikhomirov[97,*an*], Yu.A. Tikhonov[110,*c*], S. Timoshenko[99], P. Tipton[176], S. Tisserant[87], K. Todome[158], T. Todorov[5,*], S. Todorova-Nova[130], J. Tojo[72], S. Tokár[145a], K. Tokushuku[68], E. Tolley[59], L. Tomlinson[86], M. Tomoto[104], L. Tompkins[144,*ao*], K. Toms[106], B. Tong[59], E. Torrence[117], H. Torres[143], E. Torró Pastor[139], J. Toth[87,*ap*], F. Touchard[87], D.R. Tovey[140], T. Trefzger[174], A. Tricoli[27], I.M. Trigger[160a], S. Trincaz-Duvoid[82], M.F. Tripiana[13], W. Trischuk[159], B. Trocmé[57], A. Trofymov[44], C. Troncon[93a], M. Trottier-McDonald[16], M. Trovatelli[169], L. Truong[164a,164c], M. Trzebinski[41], A. Trzupek[41], J.C-L. Tseng[121], P.V. Tsiareshka[94], G. Tsipolitis[10], N. Tsirintanis[9], S. Tsiskaridze[13], V. Tsiskaridze[50], E.G. Tskhadadze[53a], K.M. Tsui[62a], I.I. Tsukerman[98], V. Tsulaia[16], S. Tsuno[68], D. Tsybychev[149], A. Tudorache[28b], V. Tudorache[28b], A.N. Tuna[59], S.A. Tupputi[22a,22b], S. Turchikhin[100,*al*], D. Turecek[129], D. Turgeman[172], R. Turra[93a,93b], A.J. Turvey[42], P.M. Tuts[37], M. Tyndel[132], G. Ucchielli[22a,22b], I. Ueda[156], R. Ueno[31], M. Ughetto[147a,147b], F. Ukegawa[161], G. Unal[32], A. Undrus[27], G. Unel[163], F.C. Ungaro[90], Y. Unno[68], C. Unverdorben[101], J. Urban[145b], P. Urquijo[90], P. Urrejola[85], G. Usai[8], A. Usanova[64], L. Vacavant[87], V. Vacek[129], B. Vachon[89], C. Valderanis[101], E. Valdes Santurio[147a,147b], N. Valencic[108], S. Valentinetti[22a,22b],

A. Valero[167], L. Valery[13], S. Valkar[130], S. Vallecorsa[51], J.A. Valls Ferrer[167], W. Van Den Wollenberg[108], P.C. Van Der Deijl[108], R. van der Geer[108], H. van der Graaf[108], N. van Eldik[153], P. van Gemmeren[6], J. Van Nieuwkoop[143], I. van Vulpen[108], M.C. van Woerden[32], M. Vanadia[133a,133b], W. Vandelli[32], R. Vanguri[123], A. Vaniachine[131], P. Vankov[108], G. Vardanyan[177], R. Vari[133a], E.W. Varnes[7], T. Varol[42], D. Varouchas[82], A. Vartapetian[8], K.E. Varvell[151], J.G. Vasquez[176], F. Vazeille[36], T. Vazquez Schroeder[89], J. Veatch[56], L.M. Veloce[159], F. Veloso[127a,127c], S. Veneziano[133a], A. Ventura[75a,75b], M. Venturi[169], N. Venturi[159], A. Venturini[25], V. Vercesi[122a], M. Verducci[133a,133b], W. Verkerke[108], J.C. Vermeulen[108], A. Vest[46,aq], M.C. Vetterli[143,d], O. Viazlo[83], I. Vichou[166], T. Vickey[140], O.E. Vickey Boeriu[140], G.H.A. Viehhauser[121], S. Viel[16], L. Vigani[121], R. Vigne[64], M. Villa[22a,22b], M. Villaplana Perez[93a,93b], E. Vilucchi[49], M.G. Vincter[31], V.B. Vinogradov[67], C. Vittori[22a,22b], I. Vivarelli[150], S. Vlachos[10], M. Vlasak[129], M. Vogel[175], P. Vokac[129], G. Volpi[125a,125b], M. Volpi[90], H. von der Schmitt[102], E. von Toerne[23], V. Vorobel[130], K. Vorobev[99], M. Vos[167], R. Voss[32], J.H. Vossebeld[76], N. Vranjes[14], M. Vranjes Milosavljevic[14], V. Vrba[128], M. Vreeswijk[108], R. Vuillermet[32], I. Vukotic[33], Z. Vykydal[129], P. Wagner[23], W. Wagner[175], H. Wahlberg[73], S. Wahrmund[46], J. Wakabayashi[104], J. Walder[74], R. Walker[101], W. Walkowiak[142], V. Wallangen[147a,147b], C. Wang[35c], C. Wang[35d,87], F. Wang[173], H. Wang[16], H. Wang[42], J. Wang[44], J. Wang[151], K. Wang[89], R. Wang[6], S.M. Wang[152], T. Wang[23], T. Wang[37], W. Wang[35b], X. Wang[176], C. Wanotayaroj[117], A. Warburton[89], C.P. Ward[30], D.R. Wardrope[80], A. Washbrook[48], P.M. Watkins[19], A.T. Watson[19], M.F. Watson[19], G. Watts[139], S. Watts[86], B.M. Waugh[80], S. Webb[85], M.S. Weber[18], S.W. Weber[174], J.S. Webster[6], A.R. Weidberg[121], B. Weinert[63], J. Weingarten[56], C. Weiser[50], H. Weits[108], P.S. Wells[32], T. Wenaus[27], T. Wengler[32], S. Wenig[32], N. Wermes[23], M. Werner[50], P. Werner[32], M. Wessels[60a], J. Wetter[162], K. Whalen[117], N.L. Whallon[139], A.M. Wharton[74], A. White[8], M.J. White[1], R. White[34b], D. Whiteson[163], F.J. Wickens[132], W. Wiedenmann[173], M. Wielers[132], P. Wienemann[23], C. Wiglesworth[38], L.A.M. Wiik-Fuchs[23], A. Wildauer[102], F. Wilk[86], H.G. Wilkens[32], H.H. Williams[123], S. Williams[108], C. Willis[92], S. Willocq[88], J.A. Wilson[19], I. Wingerter-Seez[5], F. Winklmeier[117], O.J. Winston[150], B.T. Winter[23], M. Wittgen[144], J. Wittkowski[101], S.J. Wollstadt[85], M.W. Wolter[41], H. Wolters[127a,127c], B.K. Wosiek[41], J. Wotschack[32], M.J. Woudstra[86], K.W. Wozniak[41], M. Wu[57], M. Wu[33], S.L. Wu[173], X. Wu[51], Y. Wu[91], T.R. Wyatt[86], B.M. Wynne[48], S. Xella[38], D. Xu[35a], L. Xu[27], B. Yabsley[151], S. Yacoob[146a], R. Yakabe[69], D. Yamaguchi[158], Y. Yamaguchi[119], A. Yamamoto[68], S. Yamamoto[156], T. Yamanaka[156], K. Yamauchi[104], Y. Yamazaki[69], Z. Yan[24], H. Yang[35e], H. Yang[173], Y. Yang[152], Z. Yang[15], W-M. Yao[16], Y.C. Yap[82], Y. Yasu[68], E. Yatsenko[5], K.H. Yau Wong[23], J. Ye[42], S. Ye[27], I. Yeletskikh[67], A.L. Yen[59], E. Yildirim[85], K. Yorita[171], R. Yoshida[6], K. Yoshihara[123], C. Young[144], C.J.S. Young[32], S. Youssef[24], D.R. Yu[16], J. Yu[8], J.M. Yu[91], J. Yu[66], L. Yuan[69], S.P.Y. Yuen[23], I. Yusuff[30,ar], B. Zabinski[41], R. Zaidan[35d], A.M. Zaitsev[131,ae], N. Zakharchuk[44], J. Zalieckas[15], A. Zaman[149], S. Zambito[59], L. Zanello[133a,133b], D. Zanzi[90], C. Zeitnitz[175], M. Zeman[129], A. Zemla[40a], J.C. Zeng[166], Q. Zeng[144], K. Zengel[25], O. Zenin[131], T. Ženiš[145a], D. Zerwas[118], D. Zhang[91], F. Zhang[173], G. Zhang[35b,am], H. Zhang[35c], J. Zhang[6], L. Zhang[50], R. Zhang[23], R. Zhang[35b,as], X. Zhang[35d], Z. Zhang[118], X. Zhao[42], Y. Zhao[35d], Z. Zhao[35b], A. Zhemchugov[67], J. Zhong[121], B. Zhou[91], C. Zhou[47], L. Zhou[37], L. Zhou[42], M. Zhou[149], N. Zhou[35f], C.G. Zhu[35d], H. Zhu[35a], J. Zhu[91], Y. Zhu[35b], X. Zhuang[35a], K. Zhukov[97], A. Zibell[174], D. Zieminska[63], N.I. Zimine[67], C. Zimmermann[85], S. Zimmermann[50], Z. Zinonos[56], M. Zinser[85], M. Ziolkowski[142], L. Živković[14], G. Zobernig[173], A. Zoccoli[22a,22b], M. zur Nedden[17], G. Zurzolo[105a,105b], L. Zwalinski[32].

[1] Department of Physics, University of Adelaide, Adelaide, Australia

[2] Physics Department, SUNY Albany, Albany NY, United States of America

[3] Department of Physics, University of Alberta, Edmonton AB, Canada

[4] [(a)] Department of Physics, Ankara University, Ankara; [(b)] Istanbul Aydin University, Istanbul; [(c)]

Division of Physics, TOBB University of Economics and Technology, Ankara, Turkey
[5] LAPP, CNRS/IN2P3 and Université Savoie Mont Blanc, Annecy-le-Vieux, France
[6] High Energy Physics Division, Argonne National Laboratory, Argonne IL, United States of America
[7] Department of Physics, University of Arizona, Tucson AZ, United States of America
[8] Department of Physics, The University of Texas at Arlington, Arlington TX, United States of America
[9] Physics Department, University of Athens, Athens, Greece
[10] Physics Department, National Technical University of Athens, Zografou, Greece
[11] Department of Physics, The University of Texas at Austin, Austin TX, United States of America
[12] Institute of Physics, Azerbaijan Academy of Sciences, Baku, Azerbaijan
[13] Institut de Física d'Altes Energies (IFAE), The Barcelona Institute of Science and Technology, Barcelona, Spain, Spain
[14] Institute of Physics, University of Belgrade, Belgrade, Serbia
[15] Department for Physics and Technology, University of Bergen, Bergen, Norway
[16] Physics Division, Lawrence Berkeley National Laboratory and University of California, Berkeley CA, United States of America
[17] Department of Physics, Humboldt University, Berlin, Germany
[18] Albert Einstein Center for Fundamental Physics and Laboratory for High Energy Physics, University of Bern, Bern, Switzerland
[19] School of Physics and Astronomy, University of Birmingham, Birmingham, United Kingdom
[20] [(a)] Department of Physics, Bogazici University, Istanbul; [(b)] Department of Physics Engineering, Gaziantep University, Gaziantep; [(d)] Istanbul Bilgi University, Faculty of Engineering and Natural Sciences, Istanbul,Turkey; [(e)] Bahcesehir University, Faculty of Engineering and Natural Sciences, Istanbul, Turkey, Turkey
[21] Centro de Investigaciones, Universidad Antonio Narino, Bogota, Colombia
[22] [(a)] INFN Sezione di Bologna; [(b)] Dipartimento di Fisica e Astronomia, Università di Bologna, Bologna, Italy
[23] Physikalisches Institut, University of Bonn, Bonn, Germany
[24] Department of Physics, Boston University, Boston MA, United States of America
[25] Department of Physics, Brandeis University, Waltham MA, United States of America
[26] [(a)] Universidade Federal do Rio De Janeiro COPPE/EE/IF, Rio de Janeiro; [(b)] Electrical Circuits Department, Federal University of Juiz de Fora (UFJF), Juiz de Fora; [(c)] Federal University of Sao Joao del Rei (UFSJ), Sao Joao del Rei; [(d)] Instituto de Fisica, Universidade de Sao Paulo, Sao Paulo, Brazil
[27] Physics Department, Brookhaven National Laboratory, Upton NY, United States of America
[28] [(a)] Transilvania University of Brasov, Brasov, Romania; [(b)] National Institute of Physics and Nuclear Engineering, Bucharest; [(c)] National Institute for Research and Development of Isotopic and Molecular Technologies, Physics Department, Cluj Napoca; [(d)] University Politehnica Bucharest, Bucharest; [(e)] West University in Timisoara, Timisoara, Romania
[29] Departamento de Física, Universidad de Buenos Aires, Buenos Aires, Argentina
[30] Cavendish Laboratory, University of Cambridge, Cambridge, United Kingdom
[31] Department of Physics, Carleton University, Ottawa ON, Canada
[32] CERN, Geneva, Switzerland
[33] Enrico Fermi Institute, University of Chicago, Chicago IL, United States of America
[34] [(a)] Departamento de Física, Pontificia Universidad Católica de Chile, Santiago; [(b)] Departamento de Física, Universidad Técnica Federico Santa María, Valparaíso, Chile
[35] [(a)] Institute of High Energy Physics, Chinese Academy of Sciences, Beijing; [(b)] Department of Modern Physics, University of Science and Technology of China, Anhui; [(c)] Department of Physics, Nanjing University, Jiangsu; [(d)] School of Physics, Shandong University, Shandong; [(e)] Department of

Physics and Astronomy, Shanghai Key Laboratory for Particle Physics and Cosmology, Shanghai Jiao Tong University, Shanghai; (also affiliated with PKU-CHEP); [f] Physics Department, Tsinghua University, Beijing 100084, China
[36] Laboratoire de Physique Corpusculaire, Clermont Université and Université Blaise Pascal and CNRS/IN2P3, Clermont-Ferrand, France
[37] Nevis Laboratory, Columbia University, Irvington NY, United States of America
[38] Niels Bohr Institute, University of Copenhagen, Kobenhavn, Denmark
[39] [a] INFN Gruppo Collegato di Cosenza, Laboratori Nazionali di Frascati; [b] Dipartimento di Fisica, Università della Calabria, Rende, Italy
[40] [a] AGH University of Science and Technology, Faculty of Physics and Applied Computer Science, Krakow; [b] Marian Smoluchowski Institute of Physics, Jagiellonian University, Krakow, Poland
[41] Institute of Nuclear Physics Polish Academy of Sciences, Krakow, Poland
[42] Physics Department, Southern Methodist University, Dallas TX, United States of America
[43] Physics Department, University of Texas at Dallas, Richardson TX, United States of America
[44] DESY, Hamburg and Zeuthen, Germany
[45] Institut für Experimentelle Physik IV, Technische Universität Dortmund, Dortmund, Germany
[46] Institut für Kern- und Teilchenphysik, Technische Universität Dresden, Dresden, Germany
[47] Department of Physics, Duke University, Durham NC, United States of America
[48] SUPA - School of Physics and Astronomy, University of Edinburgh, Edinburgh, United Kingdom
[49] INFN Laboratori Nazionali di Frascati, Frascati, Italy
[50] Fakultät für Mathematik und Physik, Albert-Ludwigs-Universität, Freiburg, Germany
[51] Section de Physique, Université de Genève, Geneva, Switzerland
[52] [a] INFN Sezione di Genova; [b] Dipartimento di Fisica, Università di Genova, Genova, Italy
[53] [a] E. Andronikashvili Institute of Physics, Iv. Javakhishvili Tbilisi State University, Tbilisi; [b] High Energy Physics Institute, Tbilisi State University, Tbilisi, Georgia
[54] II Physikalisches Institut, Justus-Liebig-Universität Giessen, Giessen, Germany
[55] SUPA - School of Physics and Astronomy, University of Glasgow, Glasgow, United Kingdom
[56] II Physikalisches Institut, Georg-August-Universität, Göttingen, Germany
[57] Laboratoire de Physique Subatomique et de Cosmologie, Université Grenoble-Alpes, CNRS/IN2P3, Grenoble, France
[58] Department of Physics, Hampton University, Hampton VA, United States of America
[59] Laboratory for Particle Physics and Cosmology, Harvard University, Cambridge MA, United States of America
[60] [a] Kirchhoff-Institut für Physik, Ruprecht-Karls-Universität Heidelberg, Heidelberg; [b] Physikalisches Institut, Ruprecht-Karls-Universität Heidelberg, Heidelberg; [c] ZITI Institut für technische Informatik, Ruprecht-Karls-Universität Heidelberg, Mannheim, Germany
[61] Faculty of Applied Information Science, Hiroshima Institute of Technology, Hiroshima, Japan
[62] [a] Department of Physics, The Chinese University of Hong Kong, Shatin, N.T., Hong Kong; [b] Department of Physics, The University of Hong Kong, Hong Kong; [c] Department of Physics, The Hong Kong University of Science and Technology, Clear Water Bay, Kowloon, Hong Kong, China
[63] Department of Physics, Indiana University, Bloomington IN, United States of America
[64] Institut für Astro- und Teilchenphysik, Leopold-Franzens-Universität, Innsbruck, Austria
[65] University of Iowa, Iowa City IA, United States of America
[66] Department of Physics and Astronomy, Iowa State University, Ames IA, United States of America
[67] Joint Institute for Nuclear Research, JINR Dubna, Dubna, Russia
[68] KEK, High Energy Accelerator Research Organization, Tsukuba, Japan
[69] Graduate School of Science, Kobe University, Kobe, Japan

[70] Faculty of Science, Kyoto University, Kyoto, Japan
[71] Kyoto University of Education, Kyoto, Japan
[72] Department of Physics, Kyushu University, Fukuoka, Japan
[73] Instituto de Física La Plata, Universidad Nacional de La Plata and CONICET, La Plata, Argentina
[74] Physics Department, Lancaster University, Lancaster, United Kingdom
[75] [(a)] INFN Sezione di Lecce; [(b)] Dipartimento di Matematica e Fisica, Università del Salento, Lecce, Italy
[76] Oliver Lodge Laboratory, University of Liverpool, Liverpool, United Kingdom
[77] Department of Physics, Jožef Stefan Institute and University of Ljubljana, Ljubljana, Slovenia
[78] School of Physics and Astronomy, Queen Mary University of London, London, United Kingdom
[79] Department of Physics, Royal Holloway University of London, Surrey, United Kingdom
[80] Department of Physics and Astronomy, University College London, London, United Kingdom
[81] Louisiana Tech University, Ruston LA, United States of America
[82] Laboratoire de Physique Nucléaire et de Hautes Energies, UPMC and Université Paris-Diderot and CNRS/IN2P3, Paris, France
[83] Fysiska institutionen, Lunds universitet, Lund, Sweden
[84] Departamento de Fisica Teorica C-15, Universidad Autonoma de Madrid, Madrid, Spain
[85] Institut für Physik, Universität Mainz, Mainz, Germany
[86] School of Physics and Astronomy, University of Manchester, Manchester, United Kingdom
[87] CPPM, Aix-Marseille Université and CNRS/IN2P3, Marseille, France
[88] Department of Physics, University of Massachusetts, Amherst MA, United States of America
[89] Department of Physics, McGill University, Montreal QC, Canada
[90] School of Physics, University of Melbourne, Victoria, Australia
[91] Department of Physics, The University of Michigan, Ann Arbor MI, United States of America
[92] Department of Physics and Astronomy, Michigan State University, East Lansing MI, United States of America
[93] [(a)] INFN Sezione di Milano; [(b)] Dipartimento di Fisica, Università di Milano, Milano, Italy
[94] B.I. Stepanov Institute of Physics, National Academy of Sciences of Belarus, Minsk, Republic of Belarus
[95] National Scientific and Educational Centre for Particle and High Energy Physics, Minsk, Republic of Belarus
[96] Group of Particle Physics, University of Montreal, Montreal QC, Canada
[97] P.N. Lebedev Physical Institute of the Russian Academy of Sciences, Moscow, Russia
[98] Institute for Theoretical and Experimental Physics (ITEP), Moscow, Russia
[99] National Research Nuclear University MEPhI, Moscow, Russia
[100] D.V. Skobeltsyn Institute of Nuclear Physics, M.V. Lomonosov Moscow State University, Moscow, Russia
[101] Fakultät für Physik, Ludwig-Maximilians-Universität München, München, Germany
[102] Max-Planck-Institut für Physik (Werner-Heisenberg-Institut), München, Germany
[103] Nagasaki Institute of Applied Science, Nagasaki, Japan
[104] Graduate School of Science and Kobayashi-Maskawa Institute, Nagoya University, Nagoya, Japan
[105] [(a)] INFN Sezione di Napoli; [(b)] Dipartimento di Fisica, Università di Napoli, Napoli, Italy
[106] Department of Physics and Astronomy, University of New Mexico, Albuquerque NM, United States of America
[107] Institute for Mathematics, Astrophysics and Particle Physics, Radboud University Nijmegen/Nikhef, Nijmegen, Netherlands
[108] Nikhef National Institute for Subatomic Physics and University of Amsterdam, Amsterdam,

Netherlands
[109] Department of Physics, Northern Illinois University, DeKalb IL, United States of America
[110] Budker Institute of Nuclear Physics, SB RAS, Novosibirsk, Russia
[111] Department of Physics, New York University, New York NY, United States of America
[112] Ohio State University, Columbus OH, United States of America
[113] Faculty of Science, Okayama University, Okayama, Japan
[114] Homer L. Dodge Department of Physics and Astronomy, University of Oklahoma, Norman OK, United States of America
[115] Department of Physics, Oklahoma State University, Stillwater OK, United States of America
[116] Palacký University, RCPTM, Olomouc, Czech Republic
[117] Center for High Energy Physics, University of Oregon, Eugene OR, United States of America
[118] LAL, Univ. Paris-Sud, CNRS/IN2P3, Université Paris-Saclay, Orsay, France
[119] Graduate School of Science, Osaka University, Osaka, Japan
[120] Department of Physics, University of Oslo, Oslo, Norway
[121] Department of Physics, Oxford University, Oxford, United Kingdom
[122] [(a)] INFN Sezione di Pavia; [(b)] Dipartimento di Fisica, Università di Pavia, Pavia, Italy
[123] Department of Physics, University of Pennsylvania, Philadelphia PA, United States of America
[124] National Research Centre "Kurchatov Institute" B.P.Konstantinov Petersburg Nuclear Physics Institute, St. Petersburg, Russia
[125] [(a)] INFN Sezione di Pisa; [(b)] Dipartimento di Fisica E. Fermi, Università di Pisa, Pisa, Italy
[126] Department of Physics and Astronomy, University of Pittsburgh, Pittsburgh PA, United States of America
[127] [(a)] Laboratório de Instrumentação e Física Experimental de Partículas - LIP, Lisboa; [(b)] Faculdade de Ciências, Universidade de Lisboa, Lisboa; [(c)] Department of Physics, University of Coimbra, Coimbra; [(d)] Centro de Física Nuclear da Universidade de Lisboa, Lisboa; [(e)] Departamento de Fisica, Universidade do Minho, Braga; [(f)] Departamento de Fisica Teorica y del Cosmos and CAFPE, Universidad de Granada, Granada (Spain); [(g)] Dep Fisica and CEFITEC of Faculdade de Ciencias e Tecnologia, Universidade Nova de Lisboa, Caparica, Portugal
[128] Institute of Physics, Academy of Sciences of the Czech Republic, Praha, Czech Republic
[129] Czech Technical University in Prague, Praha, Czech Republic
[130] Faculty of Mathematics and Physics, Charles University in Prague, Praha, Czech Republic
[131] State Research Center Institute for High Energy Physics (Protvino), NRC KI, Russia
[132] Particle Physics Department, Rutherford Appleton Laboratory, Didcot, United Kingdom
[133] [(a)] INFN Sezione di Roma; [(b)] Dipartimento di Fisica, Sapienza Università di Roma, Roma, Italy
[134] [(a)] INFN Sezione di Roma Tor Vergata; [(b)] Dipartimento di Fisica, Università di Roma Tor Vergata, Roma, Italy
[135] [(a)] INFN Sezione di Roma Tre; [(b)] Dipartimento di Matematica e Fisica, Università Roma Tre, Roma, Italy
[136] [(a)] Faculté des Sciences Ain Chock, Réseau Universitaire de Physique des Hautes Energies - Université Hassan II, Casablanca; [(b)] Centre National de l'Energie des Sciences Techniques Nucleaires, Rabat; [(c)] Faculté des Sciences Semlalia, Université Cadi Ayyad, LPHEA-Marrakech; [(d)] Faculté des Sciences, Université Mohamed Premier and LPTPM, Oujda; [(e)] Faculté des sciences, Université Mohammed V, Rabat, Morocco
[137] DSM/IRFU (Institut de Recherches sur les Lois Fondamentales de l'Univers), CEA Saclay (Commissariat à l'Energie Atomique et aux Energies Alternatives), Gif-sur-Yvette, France
[138] Santa Cruz Institute for Particle Physics, University of California Santa Cruz, Santa Cruz CA, United States of America

[139] Department of Physics, University of Washington, Seattle WA, United States of America
[140] Department of Physics and Astronomy, University of Sheffield, Sheffield, United Kingdom
[141] Department of Physics, Shinshu University, Nagano, Japan
[142] Fachbereich Physik, Universität Siegen, Siegen, Germany
[143] Department of Physics, Simon Fraser University, Burnaby BC, Canada
[144] SLAC National Accelerator Laboratory, Stanford CA, United States of America
[145] [(a)] Faculty of Mathematics, Physics & Informatics, Comenius University, Bratislava; [(b)] Department of Subnuclear Physics, Institute of Experimental Physics of the Slovak Academy of Sciences, Kosice, Slovak Republic
[146] [(a)] Department of Physics, University of Cape Town, Cape Town; [(b)] Department of Physics, University of Johannesburg, Johannesburg; [(c)] School of Physics, University of the Witwatersrand, Johannesburg, South Africa
[147] [(a)] Department of Physics, Stockholm University; [(b)] The Oskar Klein Centre, Stockholm, Sweden
[148] Physics Department, Royal Institute of Technology, Stockholm, Sweden
[149] Departments of Physics & Astronomy and Chemistry, Stony Brook University, Stony Brook NY, United States of America
[150] Department of Physics and Astronomy, University of Sussex, Brighton, United Kingdom
[151] School of Physics, University of Sydney, Sydney, Australia
[152] Institute of Physics, Academia Sinica, Taipei, Taiwan
[153] Department of Physics, Technion: Israel Institute of Technology, Haifa, Israel
[154] Raymond and Beverly Sackler School of Physics and Astronomy, Tel Aviv University, Tel Aviv, Israel
[155] Department of Physics, Aristotle University of Thessaloniki, Thessaloniki, Greece
[156] International Center for Elementary Particle Physics and Department of Physics, The University of Tokyo, Tokyo, Japan
[157] Graduate School of Science and Technology, Tokyo Metropolitan University, Tokyo, Japan
[158] Department of Physics, Tokyo Institute of Technology, Tokyo, Japan
[159] Department of Physics, University of Toronto, Toronto ON, Canada
[160] [(a)] TRIUMF, Vancouver BC; [(b)] Department of Physics and Astronomy, York University, Toronto ON, Canada
[161] Faculty of Pure and Applied Sciences, and Center for Integrated Research in Fundamental Science and Engineering, University of Tsukuba, Tsukuba, Japan
[162] Department of Physics and Astronomy, Tufts University, Medford MA, United States of America
[163] Department of Physics and Astronomy, University of California Irvine, Irvine CA, United States of America
[164] [(a)] INFN Gruppo Collegato di Udine, Sezione di Trieste, Udine; [(b)] ICTP, Trieste; [(c)] Dipartimento di Chimica, Fisica e Ambiente, Università di Udine, Udine, Italy
[165] Department of Physics and Astronomy, University of Uppsala, Uppsala, Sweden
[166] Department of Physics, University of Illinois, Urbana IL, United States of America
[167] Instituto de Fisica Corpuscular (IFIC) and Departamento de Fisica Atomica, Molecular y Nuclear and Departamento de Ingeniería Electrónica and Instituto de Microelectrónica de Barcelona (IMB-CNM), University of Valencia and CSIC, Valencia, Spain
[168] Department of Physics, University of British Columbia, Vancouver BC, Canada
[169] Department of Physics and Astronomy, University of Victoria, Victoria BC, Canada
[170] Department of Physics, University of Warwick, Coventry, United Kingdom
[171] Waseda University, Tokyo, Japan
[172] Department of Particle Physics, The Weizmann Institute of Science, Rehovot, Israel

[173] Department of Physics, University of Wisconsin, Madison WI, United States of America
[174] Fakultät für Physik und Astronomie, Julius-Maximilians-Universität, Würzburg, Germany
[175] Fakultät für Mathematik und Naturwissenschaften, Fachgruppe Physik, Bergische Universität Wuppertal, Wuppertal, Germany
[176] Department of Physics, Yale University, New Haven CT, United States of America
[177] Yerevan Physics Institute, Yerevan, Armenia
[178] Centre de Calcul de l'Institut National de Physique Nucléaire et de Physique des Particules (IN2P3), Villeurbanne, France
[a] Also at Department of Physics, King's College London, London, United Kingdom
[b] Also at Institute of Physics, Azerbaijan Academy of Sciences, Baku, Azerbaijan
[c] Also at Novosibirsk State University, Novosibirsk, Russia
[d] Also at TRIUMF, Vancouver BC, Canada
[e] Also at Department of Physics & Astronomy, University of Louisville, Louisville, KY, United States of America
[f] Also at Department of Physics, California State University, Fresno CA, United States of America
[g] Also at Department of Physics, University of Fribourg, Fribourg, Switzerland
[h] Also at Departament de Fisica de la Universitat Autonoma de Barcelona, Barcelona, Spain
[i] Also at Departamento de Fisica e Astronomia, Faculdade de Ciencias, Universidade do Porto, Portugal
[j] Also at Tomsk State University, Tomsk, Russia
[k] Also at Universita di Napoli Parthenope, Napoli, Italy
[l] Also at Institute of Particle Physics (IPP), Canada
[m] Also at National Institute of Physics and Nuclear Engineering, Bucharest, Romania
[n] Also at Department of Physics, St. Petersburg State Polytechnical University, St. Petersburg, Russia
[o] Also at Department of Physics, The University of Michigan, Ann Arbor MI, United States of America
[p] Also at Centre for High Performance Computing, CSIR Campus, Rosebank, Cape Town, South Africa
[q] Also at Louisiana Tech University, Ruston LA, United States of America
[r] Also at Institucio Catalana de Recerca i Estudis Avancats, ICREA, Barcelona, Spain
[s] Also at Graduate School of Science, Osaka University, Osaka, Japan
[t] Also at Department of Physics, National Tsing Hua University, Taiwan
[u] Also at Institute for Mathematics, Astrophysics and Particle Physics, Radboud University Nijmegen/Nikhef, Nijmegen, Netherlands
[v] Also at Department of Physics, The University of Texas at Austin, Austin TX, United States of America
[w] Also at Institute of Theoretical Physics, Ilia State University, Tbilisi, Georgia
[x] Also at CERN, Geneva, Switzerland
[y] Also at Georgian Technical University (GTU),Tbilisi, Georgia
[z] Also at Ochadai Academic Production, Ochanomizu University, Tokyo, Japan
[aa] Also at Manhattan College, New York NY, United States of America
[ab] Also at Hellenic Open University, Patras, Greece
[ac] Also at Academia Sinica Grid Computing, Institute of Physics, Academia Sinica, Taipei, Taiwan
[ad] Also at School of Physics, Shandong University, Shandong, China
[ae] Also at Moscow Institute of Physics and Technology State University, Dolgoprudny, Russia
[af] Also at Section de Physique, Université de Genève, Geneva, Switzerland
[ag] Also at Eotvos Lorand University, Budapest, Hungary
[ah] Also at International School for Advanced Studies (SISSA), Trieste, Italy
[ai] Also at Department of Physics and Astronomy, University of South Carolina, Columbia SC, United States of America
[aj] Also at School of Physics and Engineering, Sun Yat-sen University, Guangzhou, China

[ak] Also at Institute for Nuclear Research and Nuclear Energy (INRNE) of the Bulgarian Academy of Sciences, Sofia, Bulgaria
[al] Also at Faculty of Physics, M.V.Lomonosov Moscow State University, Moscow, Russia
[am] Also at Institute of Physics, Academia Sinica, Taipei, Taiwan
[an] Also at National Research Nuclear University MEPhI, Moscow, Russia
[ao] Also at Department of Physics, Stanford University, Stanford CA, United States of America
[ap] Also at Institute for Particle and Nuclear Physics, Wigner Research Centre for Physics, Budapest, Hungary
[aq] Also at Flensburg University of Applied Sciences, Flensburg, Germany
[ar] Also at University of Malaya, Department of Physics, Kuala Lumpur, Malaysia
[as] Also at CPPM, Aix-Marseille Université and CNRS/IN2P3, Marseille, France
[*] Deceased